2 August 2014

Volatility basis-set approach simulation of organic aerosol formation in East Asia: implications for anthropogenic-biogenic interaction and controllable amounts

H. Matsui, [1] M. Koike, [2] Y. Kondo, [2] A. Takami, [3]

J. D. Fast, [4] Y. Kanaya, [1] and M. Takigawa [1]

[1] Research Institute for Global Change, Japan Agency for Marine-Earth Science and Technology, Kanagawa, Japan

[2] Department of Earth and Planetary Science, Graduate School of Science, University of Tokyo, Tokyo, Japan

[3] National Institute for Environmental Studies, Ibaraki, Japan

[4] Pacific Northwest National Laboratory, Richland, Washington, USA.

Short title: MATSUI ET AL.: VBS OA SIMULATION IN EAST ASIA

Correspondence to: H. Matsui (matsui@jamstec.go.jp)

Submitted to Atmospheric Chemistry and Physics: 14 February, 2014

Revised following reviewer's comments: 15 July 2014

Abstract

Organic aerosol (OA) simulations using the volatility basis-set approach were made for East Asia and its outflow region. Model simulations were evaluated through comparisons with OA measured by aerosol mass spectrometers in and around Tokyo (at Komaba and Kisai in summer 2003 and 2004) and over the outflow region in East Asia (at Fukue and Hedo in spring 2009). The simulations with aging processes of organic vapors reasonably well reproduced the mass concentrations, temporal variations, and formation efficiencies of observed OA at all of the sites. As OA mass was severely underestimated in the simulations without the aging processes, the oxidations of organic vapors are essential for reasonable OA simulations over East Asia. By considering the aging processes, simulated OA concentrations increased from 0.24 to 1.28 μg m^{-3} in the boundary layer over the whole of East Asia. OA formed from the interaction of anthropogenic and biogenic sources was also enhanced by the aging processes. The fraction of controllable OA was estimated to be 87 % of total OA over the whole of East Asia, which indicated that most of the OA in our simulations were formed anthropogenically (from controllable combustion sources). A large portion of biogenic secondary OA (78 % of biogenic secondary OA) was formed through the influence of anthropogenic sources. These fractions were higher than the fraction of anthropogenic emissions. An important reason for these higher controllable fractions was higher oxidant concentrations and the resulting faster oxidation rates of OA precursors by considering anthropogenic sources. Both the amounts (from 0.18 to 1.12 μg m^{-3}) and the fraction (from 75 % to 87 %) of controllable OA were increased by aging processes of organic vapors over East Asia.

46

1. Introduction

Organic aerosol (OA) accounts for a significant mass fraction of submicron aerosols in the atmosphere (Kanakidou et al., 2005; Zhang et al., 2007) and influences the Earth's climate directly (by scattering/absorption of solar radiation) and indirectly (by modifying cloud microphysical properties) (Hallquist et al., 2009). OA is directly emitted from fossil fuel combustion, biomass burning, and other sources (primary organic aerosol, POA) or formed from the oxidation of thousands of volatile organic compounds (VOCs) in the atmosphere (secondary organic aerosol, SOA). Recent studies have shown that SOA accounts for a large fraction of OA globally (e.g., Kanakidou et al., 2005; Goldstein and Galbally, 2007; Zhang et al., 2007; de Gouw and Jimenez, 2009). However, as SOA formation processes are very complicated, estimates of the SOA burden in the atmosphere and its impact on climate and human health remain highly uncertain compared with those of other aerosols such as inorganic aerosol species (Hallquist et al., 2009). The current estimation of global SOA formation rate is about 30 – 450 Tg yr^{-1} (Hallquist et al., 2009; Heald et al., 2010; Spracklen et al., 2011).

In traditional OA models, the mass concentrations of SOA produced from individual parent VOCs (for example, isoprene and terpenes for biogenic VOCs, and benzene, toluene and xylene for anthropogenic VOCs) are calculated by using two mass-based yield coefficients and two partitioning coefficients which are estimated by fitting of laboratory experimental results (two-product approach) (Odum et al., 1996, 1997). Various global- and regional-scale simulations have been made using these coefficients (e.g., Chung and Seinfeld, 2002; Tsigaridis and Kanakidou, 2003, 2007;

Heald et al., 2005, 2008), but they have underestimated observed OA and/or SOA concentrations and formation rates in the atmosphere by roughly an order of magnitude, especially over urban regions (e.g., McKeen et al., 2007; Han et al., 2008; Matsui et al., 2009a).

More recently, a significant source of SOA was proposed by laboratory studies (e.g., Robinson et al., 2007), which found missing sources of semivolatile and intermediate volatility organic compounds (S/IVOCs) and the importance of chemical aging of S/IVOCs and VOCs in the atmosphere. Donahue et al. (2006) developed a new framework for OA modeling, the volatility basis set (VBS) approach. In the VBS, individual organic vapors are categorized to surrogate species with similar volatility, and their photochemical multigenerational oxidation and gas/particle partitioning processes are calculated. The VBS approach has recently been applied to global- and regional-scale simulations (e.g., Lane et al., 2008a, 2008b; Farina et al., 2010; Pye and Seinfeld, 2010; Jathar et al., 2011). Improvements of the agreement between oxygenated OA (OOA, thought to be analogous to SOA) observed by aerosol mass spectrometers (AMS) and simulated SOA have been reported for the air over Mexico City (Hodzic et al., 2010; Tsimpidi et al., 2010, 2011; Shrivastava et al., 2011), the United States (Ahmadov et al., 2012), and Europe (Fountoukis et al., 2011; Athanasopoulou et al., 2013).

East and Southeast Asia is one of the largest sources of aerosols in the world (e.g., Dentener et al., 2006; Bond et al., 2013). Many studies have reported impacts of Asian aerosols on regional and hemispherical scales (e.g., Ramanathan et al., 2001; Carmichael et al., 2003; Adhikary et al., 2010; Matsui et al., 2011a, 2011b, 2013a;

93 Oshima et al., 2012, 2013). Several global and regional modeling studies have
94 simulated and evaluated OA over East Asia (e.g., Heald et al., 2005; 2011; Han et al.,
95 2008; Matsui et al., 2009a; Utembe et al., 2011; Mahmud and Barsanti, 2013). Most
96 previous OA simulation studies have underestimated observed OA and SOA
97 concentrations over the region. For example, Utembe et al. (2011) evaluated their
98 global OA simulations over the outflow region in East Asia through the comparisons
99 with OA measurements during the ACE-Asia campaign. While their simulations
100 reproduced the vertical profile of observed OA mass concentrations, they
101 underestimated absolute OA mass concentrations by a factor of 5. Matsui et al.
102 (2009a) simulated OA over the urban area of Tokyo in July and August 2003. The
103 simulations reproduced the absolute concentrations and their temporal variations of
104 observed NO_x, ozone (O_3), VOCs, and inorganic aerosols reasonably well, but severely
105 underestimated observed SOA (by a factor of 5) and OA concentrations (by a factor of
106 2).

107 Few studies have focused on OA concentrations and their spatial distributions
108 over the whole of East and Southeast Asia and its outflow region (Han et al., 2008;
109 Jiang et al., 2012). They also underestimated observed OA and/or SOA concentrations
110 over China. As the VBS approach has a potential to explain realistic OA
111 concentrations over East and Southeast Asia, the application and evaluation of the VBS
112 approach to the Asian region is important to obtain a quantitative understanding of OA
113 concentrations and their spatial distributions over this region.

114 The understanding on the interaction of anthropogenic and biogenic sources is
115 also very limited over the Asian region. Anthropogenic sources may substantially

influence biogenic SOA (BSOA) formation (e.g., Carlton et al., 2010; Hoyle et al., 2011; Spracklen et al., 2011). The formation of BSOA is enhanced by anthropogenic POA, NO_x, and VOCs because they increase the concentrations of precursor VOCs, the oxidation rates of VOCs, and the particle-to-gas partitioning ratios of organic compounds (e.g., Heald et al., 2008; Tsigaridis et al., 2006; Tsigaridis and Kanakidou, 2007). Carlton et al. (2010) estimated the effect of anthropogenic emissions on BSOA formation and demonstrated that more than 50 % of the predicted BSOA concentrations were influenced by anthropogenic emissions in the eastern United States. Some global modeling studies have estimated much higher contributions from enhanced BSOA (Tsigaridis et al., 2006; Hoyle et al., 2009; Spracklen et al., 2011). As anthropogenic and biogenic emissions are both very large over East and Southeast Asia, the interaction of anthropogenic and biogenic sources and the resulting enhancement of BSOA are very important and should be examined for this region. These understandings would be useful for estimating the past, current, and future OA concentrations and their regional and hemispherical climatic impacts.

The objective of this study is to understand OA concentrations and their spatial distributions over East and Southeast Asia and its outflow region with the interaction of anthropogenic and biogenic sources. We simulate OA concentrations over East Asia and its outflow region by using a VBS model we have developed (Sect. 2), and evaluate the results through comparisons with AMS measurements conducted in and around Tokyo and over the outflow region in East Asia (Sect. 3 and 4). OA spatial distributions over East Asia are described with the importance of aging treatments in the VBS (Sect. 5.1.1). We also examine the interaction of anthropogenic and biogenic

sources in OA formation processes, such as the enhancement of BSOA formation due to aging processes of anthropogenic S/IVOCs and VOCs (Sect. 5.1.3). Finally, we estimate the contribution of anthropogenically induced (controllable) OA over East Asia and the impact of aging treatments on it (Sect. 5.2). The abbreviations of organic vapors and aerosols used in this study are summarized in Table 1.

2. Regional three-dimensional model

2.1. WRF-chem model

In this study, we use the Weather Research and Forecasting/Chemistry (WRF-chem) model with the MOSAIC aerosol module (version 3.4) (Skamarock et al., 2008; Grell et al., 2005; Fast et al., 2006; Zaveri et al., 2008), which has been used in our previous studies (Matsui et al., 2009b, 2010, 2011c, 2013b, 2013c), with modifications of the schemes related to organic aerosol formation (see Sect. 2.2). The chemical processes considered in the original WRF-chem model are emissions of gaseous and aerosol species, gas-phase chemistry (Zaveri and Peters, 1999), new particle formation (Wexler et al., 1994), dynamical gas-particle partitioning (condensation/evaporation) (Zaveri et al., 2005a, 2005b, 2008), Brownian coagulation (Jacobson et al., 1994), aerosol activation (Abdul-Razzak and Ghan, 2000), aqueous-phase chemistry for inorganic species (Fahey and Pandis, 2001), and dry and wet deposition (Easter et al., 2004). The mass (sulfate (SO_4), nitrate, ammonium, black carbon (BC), POA, dust, sodium, chloride, and aerosol water) and number concentrations of aerosols are explicitly calculated for the size range from 40 nm to 10 μm in 8 size bins. The meteorological and chemical process options adopted in this

study are summarized in Table 2. More detailed descriptions of the WRF-chem/MOSAIC model are given elsewhere (Fast et al., 2006).

2.2. OA formation scheme (VBS)

The WRF-chem model was modified to consider OA formation processes using the VBS approach (Fig. 1). Table 3 shows the summary of the OA formation scheme developed in this study. Similar to previous studies (e.g., Lane et al., 2008a; Tsimpidi et al., 2010, Shrivastava et al., 2011), this study uses 9 surrogate volatility species to represent S/IVOCs with effective saturation concentrations (C*, saturation concentrations at 300K) of 10^{-2}, 10^{-1}, 1, 10, 10^{2}, 10^{3}, 10^{4}, 10^{5}, and 10^{6} μg m^{-3}. Gas-phase chemistry is represented by the SAPRC99 mechanism (Carter, 2000) with the formation of first-generation oxidized VOCs (OVOCs) from the 9 lumped VOCs; alkanes (ALK4 and ALK5), olefins (OLE1 and OLE2), aromatics (ARO1 and ARO2), isoprene (ISOP), monoterpene (TERP), and sesquiterpene (SESQ). The mass yields of the OVOCs from each lumped VOC are calculated using the same NO_x-dependent 4-product basis fit (C* of 1, 10, 100, and 1000 μg m^{-3}) used by Tsimpidi et al. (2010). S/IVOCs and OVOCs are oxidized to the surrogate species with an order of magnitude lower C* by OH radical with an assumed rate constant of 1×10^{-11} cm^3 $molecule^{-1}$ s^{-1} (Fig. 1). The increase in SOA mass due to the addition of an oxygen atom is taken into account, as described by Tsimpidi et al. (2010): 7.5% increase for the reduction of volatility by one order of magnitude. The enthalpy of vaporization is based on Tsimipidi et al. (2010) and Lane et al. (2008a): 64 – 112 kJ mol^{-1} for POA and 30 kJ mol^{-1} for SOA. Our scheme traces 53 surrogate vapor species (9 for primary S/IVOCs,

185 8 for oxygenated S/IVOCs, and 36 for OVOCs) and the corresponding 53 aerosol
186 species for bulk aerosol mass concentrations. In this study, we define oxidized POA
187 (OPOA) as OA from oxygenated S/IVOCs, anthropogenic SOA (ASOA) as OA from
188 anthropogenic VOCs (ALK4, ALK5, OLE1, OLE2, ARO1, and ARO2), and biogenic
189 SOA (BSOA) as OA from biogenic VOCs (ISOP, TERP, and SESQ) (Fig. 1).

190 The scheme assumes equilibrium between the vapor and particulate species.
191 Bulk equilibrium gas-particle partitioning is calculated with an iteration scheme of
192 Schell et al. (2001). The changes in size-resolved mass concentrations in the 8 size
193 bins are calculated based on Koo et al. (2003) with the Kelvin effect. The fraction of
194 total flux of species *i* between gas and aerosol phases that condenses onto or evaporates
195 from aerosol size bin *k* ($f_{i,k}$) is given by

196

197 $$f_{i,k} = \frac{2\pi N_k d_k D_i F(C_i - C_i^{eq}\eta)}{\sum_k 2\pi N_k d_k D_i F(C_i - C_i^{eq}\eta)} \quad (1)$$

198

199 where N_k is the number concentrations in bin k, d_k is the mean diameter of bin k, D_i, C_i,
200 and C_i^{eq} are the diffusivity, bulk gas-phase concentration, and equilibrium concentration
201 at the particle surface of species i, respectively, F is the correction for the
202 non-continuum effects which depends on the Knudsen number and the accommodation
203 coefficient (we assume a value of 0.1, which has been used in previous studies (Zhang
204 et al., 2004; Zaveri et al., 2008)), and η is the Kelvin effect correction. In our scheme,
205 equation (1) is calculated for individual VBS species (53 species), but all of the
206 size-resolved information is not directly used to calculate the three-dimensional
207 transport processes to reduce the computational cost. Only total OA (sum of all VBS

208 species) is transported with the size-resolved information, and individual VBS species
209 are transported with the information of bulk mass concentrations only (not size-resolved
210 and we assume that all VBS species have the same size distribution). This treatment
211 can reduce the number of transport variables (therefore computational cost) by a factor
212 of 4 compared with the size-resolved treatment for all VBS species and by a factor of 3
213 compared with the 4-bin scheme presented in Shrivastava et al. (2011), which was
214 implemented in the original WRF-chem model (Table 3). Therefore, the scheme
215 developed in this study is a detailed (9 species), size-resolved (for total OA), and
216 computationally efficient VBS scheme.

217 In WRF-chem, interstitial (aerosol-phase) and in-cloud (cloud-phase) aerosols
218 are treated separately for all aerosol species (5 inorganic species, BC, OA, and dust) and
219 size bins to calculate in-cloud aerosol formation, regeneration, and wet removal
220 processes. Therefore, OA size distribution is calculated separately for aerosol-phase
221 and cloud-phase in our model. The model considers the increase in total OA (sum of
222 all VBS species) through aerosol regeneration after cloud evaporation. As the
223 information of each VBS species is not calculated for in-cloud aerosols in our model,
224 the chemical compositions (mass fraction of each VBS species) of regenerated OA are
225 assumed to equal those of interstitial OA at the same three-dimensional grid cell.

226 The emission factors of S/IVOCs and POA were assumed based on Shrivastava
227 et al. (2011). In this study, we applied the factors for anthropogenic sources (Table 2
228 of Shrivastava et al. (2011)) to all the emission sources. The sum of all S/IVOCs and
229 POA emissions is 7.5 times the traditional POA emissions (Fig. 1), which are based on
230 the rough estimate of the SVOC/POA ratio of 3 and the IVOC/SVOC ratio of 1.5 (or the

231 IVOC/POA ratio of 4.5) in previous studies (Tsimpidi et al., 2010; Shrivastava et al.,
232 2011). To ensure consistent aerosol number concentrations between the traditional OA
233 emissions and the S/IVOCs/POA emissions, we assume particulate emissions (POA) for
234 C* ranging from 10^{-2} to 1 μg m^{-3}, gas-phase emissions (S/IVOCs) for C* ranging from
235 10^{6} to 10^{2} μg m^{-3}, and a mixture of gas-phase and particulate emissions for C* of 10 μg
236 m^{-3} (Fig. 1).

237 Dry deposition of organic vapors (S/IVOCs and OVOCs) is calculated by the
238 scheme of Wesely (1989), which is used in the original WRF-chem/MOSAIC model.
239 In this study, the dry deposition velocity of HNO_3 is assumed for all of the organic
240 vapors, which is consistent with Ahmadov et al. (2012). Dry deposition of OA is
241 calculated for each size bin with the scheme used in the original WRF-chem model
242 (Binkowski and Shankar, 1995; Easter et al., 2004). In-cloud scavenging of organic
243 vapors (S/IVOCs and OVOCs) is calculated by assuming an aqueous-phase fraction of
244 unity (all organic vapors are soluble). Below cloud scavenging of organic vapors is
245 calculated by assuming the mass transfer rate of HNO_3 to rain given in Levine and
246 Schwarz (1982). In-cloud and below cloud scavenging of OA are calculated for each
247 size bin as calculated in the original WRF-chem model (Easter et al., 2004). A
248 hygroscopicity value (κ) of 0.14, which is the value used in the original WRF-chem for
249 POA, is assumed for all OA species used in the VBS.

250 In our VBS model, oxidation processes are considered only for gaseous species,
251 namely, homogenous aging by OH radical. Our model does not consider other
252 processes, such as aqueous-phase reactions (e.g., Ervens et al., 2011; Liu et al., 2012),
253 heterogeneous oxidation (e.g., George et al., 2007, 2008), oligomerization (e.g.,

Kalberer et al., 2004; Iinuma et al., 2004), and fragmentation (e.g., Jimenez et al., 2009; Kroll et al., 2009; Murphy et al., 2012). These processes could be important because they alter the volatility and oxidation state (i.e., an atomic O/C ratio) of organic vapors and OA, which leads to changes in OA concentrations. However, these processes currently have large uncertainties regarding their in reaction rates and products (Hallquist et al., 2009). Some recent studies have developed two-dimensional VBS schemes (2D-VBS) in which the volatility and oxidation state were calculated by considering functionalization and fragmentation (e.g., Jimenez et al., 2009; Donahue et al., 2011; Murphy et al., 2011, 2012; Shrivastava et al., 2013). In Murphy et al. (2012), heterogeneous oxidation and aqueous-phase chemistry processes were also taken into account. They applied their one-dimensional (column) chemical transport model to Europe and showed that the simple one-dimensional (volatility only) VBS (1D-VBS) scheme reproduced observed OA mass concentrations and O/C ratios reasonably well and that the performance of the 1D-VBS scheme was not worse than that of their more complex 2D-VBS schemes, likely due to the uncertainties in understanding of SOA evolution in the atmosphere. Considering these uncertainties and computational costs of complex 2D-VBS schemes, we use a simpler 1D-VBS scheme in this study.

2.3. Uncertainties in the treatment of the VBS model

To understand the uncertainties of the simplicity in our VBS model, we conducted a sensitivity simulation without the simplicity. In this simulation, OA size distribution is calculated for each VBS species (53 species × 8 size bins). Aerosol-phase and cloud-phase aerosols and their size distributions are calculated

277 separately for each VBS species. From the comparison between the sensitivity
278 simulation including the full representations of OA species and the base case simulation,
279 the uncertainties in the estimation of SOA mass concentrations in the base simulation
280 were estimated to be about 20% (as a total effect of OA formation, activation, and
281 removal processes). The correlation coefficient (R^2) of SOA spatial distribution (at
282 about 1 km) between the two simulations was 0.96, suggesting that the performance of
283 the OA distributions is sufficient in the base case simulation.

284 Our VBS scheme includes large uncertainties in the treatments of aging
285 parameters, emission factors, and dry and wet deposition of organic vapors, which could
286 change simulated OA concentrations considerably. In this study, the sensitivity of
287 aging coefficients is examined in Sect. 4.2 and 5.1.2. The uncertainties in the emission
288 factors and the treatments of dry and wet deposition for organic vapors used in the VBS
289 scheme are briefly described here. The S/IVOCs-to-POA emission ratio of 7.5 that
290 was used in this study is a highly uncertain parameter. A sensitivity simulation with an
291 increase in SVOC (C* ranging from 10^3 to 10^{-2} μg m^{-3}) emissions by a factor of 2
292 enhanced total OA and SOA concentrations by 25% and 45%, respectively, in our
293 application over East Asia (period- and domain-averaged values at an altitude of about 1
294 km). Another sensitivity simulation with an increase in IVOC (C* ranging from 10^6 to
295 10^4 μg m^{-3}) emissions by a factor of 2 enhanced total OA and SOA concentrations by
296 20% and 15%, respectively. These results suggest that OA concentrations are
297 moderately sensitive to the treatment of S/IVOC emissions over East Asia. OA
298 concentrations are sensitive to the dry deposition treatment of organic vapors because a
299 factor of 2 different velocities for S/IVOCs and OVOCs lead to an increase/decrease in

OA concentrations about 50% in our application over East Asia. OA concentrations are also moderately sensitive to the wet deposition treatment of S/IVOCs and OVOCs. OA concentrations were increased by 25% in the simulation without wet deposition of S/IVOCs and OVOCs.

3. Measurements and simulation setups

In this study, we simulate OA formation both in and around Tokyo urban area (Sect. 3.1) and over East Asia (Sect. 3.2). The purpose of the simulation in and around Tokyo is to validate the VBS scheme over the region where meteorological fields, emissions, and the concentrations of precursor gaseous species are relatively well known (compared with over the Asian region). We used observed data during the Integrated Measurement Program for Aerosol and oxidant Chemistry in Tokyo (IMPACT) campaign (Takegawa et al., 2006a, 2006b; Kondo et al., 2006, 2007, 2008, 2010). OA mass concentrations observed with an Aerodyne AMS and gaseous species such as O_3, OH, and VOCs are available for the campaign period. These data can be used to validate the simulations and constrain the parameters related to OA formation such as precursor VOCs. The simulation over Asia is conducted to understand the behavior of OA over all of East and Southeast Asia and its outflow region, though there are uncertainties in emissions and limitations of validations especially for precursor gases. OA mass concentrations (Aerodyne AMS) at two sites in Japan were used to evaluate the simulations over the outflow regions from the Asian continent.

3.1. Simulation in and around Tokyo (summer 2003 and 2004)

We used OA mass concentrations observed by an Aerodyne AMS and gaseous species of O_3 and VOCs at an urban area, Komaba (35.66°N, 139.67°E), Tokyo, in July and August 2003 during the IMPACT-2 campaign and at a suburban site, Kisai (36.08°N, 139.55°E), Saitama, in July and August 2004 during the IMPACT-L campaign (Fig. 2a). Details of the measurements are given elsewhere (Takegawa et al., 2005, 2006a, 2006b; Kondo et al., 2006, 2007, 2008, 2010, Shirai et al., 2007; Kanaya et al., 2007).

The oxygenated and hydrocarbon-like OA concentrations (OOA and HOA) were estimated by least-squares fits to the time series of OA using a linear combination of the time series of AMS-derived signals at the mass-to-charge (m/z) ratios of 44 and 57 (Zhang et al., 2005). Though there are some uncertainties in this method, the OOA/HOA concentrations derived from this method can be used as a proxy for SOA/POA concentrations because SOA and POA concentrations, which were estimated from the correlation of total OA with CO, correlated well with HOA and OOA, with slopes of 0.88–1.36 (R^2 of 0.76 – 0.85) and 0.97–1.41 (R^2 of 0.65 – 0.85), respectively, during the IMPACT campaign (Takegawa et al., 2006a, 2006b; Kondo et al., 2007). We used observed HOA concentrations to constrain POA emissions and to simulate realistic POA concentrations by the model (see below). Observed OOA is used to validate simulated SOA (Sect. 4.1).

For the simulations in and around Tokyo, the horizontal grid spacings in the model domain are 27 km (outer domain) and 9 km (inner domain) (horizontal scale of 9 × 7 degrees, Fig. 2a), and there are 18 vertical levels from the surface to 100 hPa. The lowest layer is about 30 m in depth. The simulation periods are 17 July – 15 August 2003 during the IMPACT-2 campaign and 23 July – 15 August 2004 during the

346 IMPACT-L campaign. The first 2 days of data were used for model spin-up. The
347 National Centers for Environmental Prediction (NCEP) Final (FNL) Operational Global
348 Analysis data were used for initial and boundary conditions and nudging (free
349 troposphere only) of meteorological fields. We made two model simulations, with and
350 without aging processes of organic vapors in the VBS.

351 We used anthropogenic emission inventories for 1998 at a horizontal resolution
352 of 10 × 10 km^2 with seasonal and diurnal dependencies (Kannari et al., 2004). The
353 detailed description of the inventories is given by Matsui et al. (2009a). We also used
354 on-line biogenic emissions: the Model of Emissions of Gases and Aerosols from Nature
355 version 2 (MEGAN2) (Guenther et al., 2006). Using the same approach as described
356 in Matsui et al. (2009a), the emissions of aromatics (toluene and xylene) and POA were
357 increased or decreased over all of the simulation domains (without modification of the
358 spatial emission patterns) to achieve good agreement between the observed and
359 simulated mean concentrations of these species at the Komaba site during the
360 IMPACT-2 campaign: ARO1 (toluene-like) and ARO2 (xylene-like) emissions were
361 reduced by 50% and 30%, respectively, and POA emissions were increased by 25%.
362 As the simulations with these modifications can reproduce mean concentrations of
363 aromatics and POA during the simulation period, at least at and around Komaba, we can
364 robustly evaluate the performance of OA formation processes. The modifications of
365 emissions were applied to the simulations in and around Tokyo only. We did not use
366 these modifications in the simulations over East Asia (section 3.2).

367

368 **3.2. Simulation over East Asia (spring 2009)**

We used OA and sulfate mass concentrations observed with an Aerodyne AMS at Fukue (32.75°N, 128.68°E) and Hedo (26.87°N, 128.25°E), Japan, in March and April 2009 during the Aerosol Radiative Forcing in East Asia (A-FORCE) aircraft campaign (Oshima et al., 2012). As described by Takami et al. (2005, 2007), the collection efficiency was assumed to be 0.5 at Fukue and 1.0 at Hedo. Details of the AMS measurements at Fukue and Hedo are described by Takami et al. (2005, 2007). OA measurements over the outflow regions in East Asia are limited and are useful for evaluating the model simulations. The air parcels observed at Fukue and Hedo represent the histories of sources from wide areas over northern China and their histories during transport (e.g., Kondo et al., 2011; Matsui et al., 2013a), which suggests that model evaluations at these sites are suitable for the overall validations of aerosol sources, transport, and transformation from the Asian continent to the Pacific. We also used BC mass concentrations observed with a continuous soot monitoring system (COSMOS) to evaluate primary aerosols at Fukue and Hedo (Kondo et al., 2011).

For the simulation over East Asia, the horizontal grid spacings for the model domain are 180 km (outer domain) and 60 km (inner domain) (horizontal scale of 120 × 60 degrees, Fig. 2b), and there are 26 vertical levels from the surface to 100 hPa. The lowest layer is about 30 m in depth. The simulation period is 21 March – 26 April 2009 during the A-FORCE aircraft campaign. The statistics are calculated for 24 March – 26 April 2009 period. The NCEP-FNL data were used for initial and boundary conditions and nudging (free troposphere only) of meteorological fields. Our previous simulations using WRF-chem successfully reproduced meteorological fields due to synoptic-scale meteorological variations and related transport and variation

processes of aerosol mass and number concentrations observed by both the aircraft and surface measurements during the A-FORCE period (Matsui et al., 2013b, 2013c). Our previous simulation using similar model settings also showed that the observed precipitation and its spatial distributions were generally reproduced by WRF during the simulation period (Oshima et al., 2013). Table 4 shows a list of the simulations over East Asia conducted in this study.

We used the anthropogenic and volcanic emission inventories of Streets et al. (2003), which were also used in our previous studies (Matsui et al., 2013b, 2013c). SO_2 emissions from the Miyakejima volcano were modified based on measurements, as shown by Matsui et al. (2013c). We also used daily biomass burning emissions from the Global Fire Emissions Database version 3 (GFED3) (van der Werf et al., 2010), and on-line biogenic emissions from MEGAN2. Sea salt and dust emissions from natural sources are not considered in this study.

Anthropogenic POA (from fossil fuel and biofuel combustion) is emitted mostly from China and India (Fig. 3a), while biomass burning POA is emitted mainly from Southeast Asia and Siberia (Fig. 3b). Anthropogenic and biomass burning sources account for 69 % and 31 % of total POA emissions, respectively. ARO1 (anthropogenic) emissions are distributed over China, India, Southeast Asia, Japan, and South Korea (Fig. 3c). The main source regions of TERP (biogenic) are Southeast Asia and southern China (Fig. 3d).

4. Model results and evaluation

4.1. IMPACT campaign (Tokyo)

Figures 4a and b show the time-series of O_3 and SOA at Kisai during the IMPACT-L campaign (25 July – 15 August 2004). Simulated SOA is the sum of OPOA, ASOA, and BSOA. Simulated concentrations in Sect. 4 were chosen from a grid cell closest to each measurement site and were calculated for particles with diameters of less than 1 μm. The data at the lowest layer were chosen for comparison with the surface measurements. Meteorological conditions during the campaign are summarized by Takegawa et al. (2006a). Northerly and easterly winds were dominant during 25 – 30 July, persistent southerly winds were dominant during 31 July – 9 August (associated with a stable anticyclone located east of Tokyo), and the sea-land breeze circulation was dominant during 10 – 14 August (associated with a stable anticyclone over Tokyo). Due to these meteorological conditions, relatively fresh air was transported from the Tokyo metropolitan area to Kisai by 9 August, which resulted in relatively low O_3 and SOA concentrations at Kisai. In contrast, stagnant and aged air was transported to Kisai during 10 – 14 August, which enhanced O_3 and SOA concentrations at Kisai due to the accumulation of pollutants.

The simulation reproduces the absolute concentrations and the diurnal and day-to-day variations of observed O_3 and SOA concentrations reasonably well (Fig. 4 and Table 5). In particular, the model reproduces the contrast between the early (25 July – 6 August, low concentrations) and the later (7 – 15 August, high concentrations) simulation periods and the diurnal peak concentrations of both O_3 and SOA (Fig. 4). The daytime peak concentrations of OH and HO_2 radicals are also reproduced by within 50% at Komaba during the IMPACT-L campaign in our simulations, though the concentrations have large day-to-day variability: the median values of the daytime peak

438 concentrations of observed OH and HO_2 were 6.3×10^6 cm^{-3} and 5.7 pptv, respectively
439 (Kanaya et al., 2007), and those of simulated OH and HO_2 were 9.8×10^6 cm^{-3} and 6.8
440 pptv, respectively.

441 As both O_3 and SOA were produced by photochemical reactions during the
442 IMPACT-2 and IMPACT-L campaigns, the SOA/O_3 ratio can be used as an index of OA
443 formation efficiency under given oxidative conditions (Fig. 5) (Herndon et al., 2008;
444 Kondo et al., 2008). The model simulation tends to overestimate maximum SOA
445 concentrations during daytime and underestimate SOA concentrations during nighttime.
446 However, mean SOA concentrations are reproduced by the model to within 25 % of the
447 corresponding observed values (underestimations of 21 % and 13 % during the
448 IMPACT-2 and IMPACT-L campaigns, respectively) (Table 5). In both campaigns, the
449 simulated fitting slopes (with aging processes) are consistent with the observed slopes
450 (and hence, OA formation efficiency): the observed and simulated fitting slopes are 0.16
451 and 0.19, respectively, during the IMPACT-2 campaign and 0.15 and 0.20, respectively,
452 during the IMPACT-L campaign.

453 The simulation without aging processes (orange lines and triangles in Fig. 4
454 and 5), which is similar to the simulation using a traditional OA model, severely
455 underestimates mean observed OA concentrations by 76 % and 86 % and fitting slopes
456 by 80 % and 82 % during the IMPACT-2 and IMPACT-L campaigns, respectively.
457 These results show that the emissions of S/IVOCs and the oxidation processes of
458 organic vapors (S/IVOCs and OVOCs) must be considered for reasonable OA
459 simulations in and around Tokyo: including these in the VBS scheme considerably
460 improved the model's ability to simulate OA absolute concentrations and their temporal

461 variations in Tokyo and its outflow area at Kisai.

462 In our simulations, SOA is formed mainly from anthropogenic sources at
463 Komaba and Kisai (77 – 80% of total SOA). The three largest precursors of SOA are
464 aromatics (ARO1 and ARO2, 48%), olefins (OLE1 and OLE2, 13 – 18%), and
465 monoterpenes (TERP, 13 – 16%). OPOA accounts for only 6 – 7% of total SOA at
466 both sites during the simulation periods.

467

468 **4.2. A-FORCE periods (East Asia)**

469 Figures 6a-6d show the time-series of BC and SO_4 at the Fukue and Hedo sites
470 during the A-FORCE campaign (24 March – 26 April 2009). The meteorological
471 conditions during this period are described by Matsui et al. (2013b, 2013c).
472 Synoptic-scale meteorological variations controlled temporal variations of observed
473 aerosol concentrations at Fukue and Hedo: high concentrations during the period
474 covered by a high-pressure system and rapid decreases in concentrations after the
475 passage of a cold front. At Fukue, the site was covered by a high pressure system
476 during the middle of the simulation period (6 – 12 April), and cold fronts passed on 14,
477 20, and 24 April. The temporal variations of observed BC and SO_4 due to
478 synoptic-scale meteorological variations are generally reproduced by the model
479 simulation. The mean BC concentrations are reproduced well by the model at Fukue
480 and Hedo (normalized mean bias (NMB) of -14% at Fukue and -24% at Hedo). The
481 mean SO_4 concentrations at Fukue are also reproduced well by the model (NMB of
482 -11%, Table 5), while those at Hedo are overestimated by a factor of 2 during the middle
483 and latter parts of the simulation period (NMB of 78%, Table 5).

484 Figures 6e and 6f show the time-series of OA at Fukue and Hedo during the
485 A-FORCE period. At both sites, most of the measured OA was OOA and most of the
486 simulated OA was SOA (shown below). The temporal variations of OA are generally
487 similar to those of SO_4 at both sites. At Fukue, the model overestimates OA
488 concentrations during 7 – 15 April but underestimates them during 28 March – 2 April.
489 The model well reproduces observed OA concentrations during the other periods. The
490 period-averaged OA concentrations are slightly overestimated (NMB of 12%, Table 5),
491 but the model simulations agree well with the measurements.
492 At Hedo, simulated OA concentrations are overestimated by 80% (Table 5).
493 The period of OA overestimation corresponds to the period of SO_4 overestimation.
494 Therefore, it is unlikely that the problems in OA formation processes are the only
495 factors that made the discrepancy between observed and simulated OA concentrations.
496 The model may overestimate the transport of pollutants, including precursor species and
497 secondary aerosol formation from them. The uncertainties in the AMS measurements
498 may also contribute to the discrepancy between the measurements and model
499 simulations because the observed OA concentrations at Hedo are the lower limit in
500 terms of the collection efficiency (section 3.2).
501 Observed OOA/OA ratio was estimated to be greater than 95% at Fukue and
502 Hedo (Zhang et al., 2007). Simulated SOA/OA ratio is 84% at Fukue and 83% at
503 Hedo, suggesting that our model simulations tend to underestimate the fraction of SOA
504 to total OA at these measurement sites.
505 Figures 6g and 6h show the time-series of OA/SO_4 ratio at Fukue and Hedo
506 during the A-FORCE period. The OA/SO_4 ratio is used because both OA and SO_4 at

these sites are formed through oxidation processes in the atmosphere. Their oxidation pathways may not be the same (OA is formed from gas-phase oxidation only, but SO_4 is formed from both gas-phase and aqueous-phase oxidation in our model), but as the formation processes of SO_4 are relatively well known compared with those of OA, the OA/SO_4 ratio can be used as an index of OA formation efficiency relative to the amounts of secondary aerosols transported to the measurement sites. The model reproduces reasonably well the period-averaged OA/SO_4 ratio observed at Fukue and Hedo: the observed ratios are 0.89 and 0.58, and the simulated ratios are 0.78 (NMB of -12%) and 0.42 (NMB of -30%), respectively (Table 5).

In contrast, the simulation without aging processes do not capture observed OA mass concentrations and OA/SO_4 ratios. The model without aging processes considerably underestimates both the OA concentrations (by 88% and 83%) and the OA/SO_4 ratio (by 85% and 90%) at Fukue and Hedo, respectively. These results demonstrate that the VBS scheme with aging processes much improves the model performance; the scheme realistically simulated OA mass concentrations and their temporal variations and the OA/SO_4 ratio over the outflow regions in East Asia.

Simulated SOA is formed mostly from anthropogenic sources at Fukue and Hedo (90 – 91% of total SOA). The three largest sources are aromatics (ARO1 and ARO2, 41 – 46%), S/IVOCs (34 – 41%), and monoterpenes (TERP, 7 – 8%). The contributions of OPOA at Fukue and Hedo (34 – 41% of total SOA) are much higher than those at Komaba and Kisai (6 – 7% of total SOA), due to continuous aging processes of organic vapors during transport from source areas to the measurement sites at Fukue and Hedo.

530 The uncertainties in the aging coefficients of S/IVOCs are very large in the
531 VBS scheme. To understand the impact of these uncertainties on simulated OA mass
532 concentrations, we conducted sensitivity simulations using aging coefficients of 4 ×
533 10^{-11} cm^3 $molecule^{-1}$ s^{-1} (4 times of the base case, "Aging-4") and 2.5 × 10^{-12} cm^3
534 $molecule^{-1}$ s^{-1} (1/4 of the base case, "Aging-0.25") (Fig. 6e and 6f, Table 4). The
535 Aging-4 (Aging-0.25) simulation increased (decreased) period-averaged OA mass
536 concentrations by factors of 3.2 (2.1) and 4.1 (2.4) at Fukue and Hedo, respectively;
537 thus simulated OA concentrations over East Asia are greatly affected by the choice of
538 aging coefficients. Therefore, it is important to improve our understanding of the
539 oxidation processes of organic vapors by using laboratory and field measurements and
540 by applying and validating the VBS scheme for various atmospheric conditions.
541
542 **5. Spatial distribution of OA over East Asia**
543 **5.1. Impact of aging processes**
544 **5.1.1. Mass concentrations and contributions**
545 Next, we examine the spatial distributions of OA over East Asia. In Sect. 5,
546 all particles between 40 nm and 10 μm in diameter were used to calculate OA
547 concentrations. For the simulation with the aging process, POA concentrations at an
548 altitude of about 1 km peak over Southeast Asia and northern and central China (Fig.
549 7a), corresponding to large source regions of biomass burning and anthropogenic
550 emissions, respectively (Fig. 3a and b). The spatial distribution of OPOA is similar to
551 that of POA (Fig. 7c). ASOA concentrations are high over northern and central China
552 and moderate over southern China, Japan, and Southeast Asia (Fig. 7e). The

553 maximum of BSOA concentration is over Southeast Asia and southern China (Fig. 7g).
554 Total SOA (OPOA + ASOA + BSOA) concentrations are distributed widely over East
555 Asia with peaks over Southeast Asia and northern and central China (Fig. 7i).

556 The large contribution of BSOA over southern China and Southeast Asia is
557 consistent, at least qualitatively, with previous OA modeling studies (Han et al., 2008;
558 Jiang et al., 2012; Li et al., 2013), in which 65 – 90 % of SOA in southern China was
559 estimated to be biogenic. Several measurement studies have reported mean organic
560 carbon (OC) concentrations in spring over Guangzhou in southern China of 6 – 7 μg m^{-3}
561 (Tao et al., 2012; Huang et al., 2012), over Hong Kong of 6 – 9 μg m^{-3} (Bahadur et al.,
562 2009), and over Bangkok of about 10 μg m^{-3} (Sahu et al., 2011). We compared our
563 simulation results with these measurements, though the meteorological conditions, the
564 amounts of emissions (e.g., biomass burning, biogenic), or both may have differed
565 between those studies and ours. When we assume an OC-to-OA conversion rate of 1.6
566 (Turpin and Lim, 2001), our simulations underestimate observed OA concentrations by
567 35% at Guangzou and by 60 – 70% at Hong Kong and Bangkok. OOA concentrations
568 in the Pearl River Delta region observed with an AMS have also been reported: about 5
569 μg m^{-3} in summer 2006 (Xiao et al., 2011) and in fall 2009 (Li et al., 2013). Our
570 simulations underestimate the observed SOA concentrations by 30 – 40% in this region.
571 The rough comparisons shown above suggest that our OA and SOA simulations over
572 southern China and Southeast Asia are consistent with measurements within a factor of
573 3 (underestimation by 30 – 70%). The agreement between the measurements and
574 model simulations over southern China and Southeast Asia was much improved by
575 considering aging processes of organic vapors in the VBS scheme.

SOA concentrations in the Aging-off simulation are much lower than those in the Aging-on simulation (Fig. 7). By considering aging processes, ASOA, BSOA, OPOA, total SOA, and total OA concentrations increased by between 440% and 1380% over the outer domain (Fig. 8a and Table 6), demonstrating the importance of aging processes in OA simulations for East Asia. POA concentrations, however, vary less: the Aging-on POA concentrations over the outer domain are about 30% more than those for the Aging-off simulations (Fig. 8a and Table 6). The lower POA concentrations in the Aging-off simulation are likely due to the smaller amounts of low-volatile organic vapors, which are produced by OH oxidation in the Aging-on simulation, and the resulting reduction of OA concentrations in the particulate phase due to the shift of the gas-particle partitioning to the gas-phase.

In addition to differences in the absolute mass concentrations, the contributions from individual chemical compositions to total OA also differ greatly between the Aging-on and Aging-off simulations (Fig. 8b and c). In the Aging-on simulation, POA, OPOA, ASOA, and BSOA account for 18%, 29%, 26%, and 27% of OA, respectively, over the outer domain. The main precursors of ASOA are aromatics (ARO1 and ARO2, 80% of ASOA), and those of BSOA are monoterpenes (TERP, 55% of BSOA). In the aging-off simulation, POA is dominant (70% of total OA) due to the formation of much lower concentrations of ASOA and BSOA with no OPOA.

5.1.2. Sensitivity of aging parameters over East Asia

Table 6 shows the results of the Aging-4 and Aging-0.25 simulations. Similar to the results at Fukue and Hedo (Sect. 4.2), SOA concentrations are highly sensitive to

599 aging coefficients over the simulation domain. The period-averaged mass
600 concentrations of OPOA, ASOA, and BSOA were enhanced (reduced) by factors of 3.3
601 (6.6), 2.0 (3.1), and 1.9 (2.6), respectively, in the Aging-4 (Aging-0.25) simulation over
602 the whole East Asian region (Table 6a). In contrast, POA concentrations are not so
603 sensitive to the aging coefficients. The average POA concentrations increased by 17%
604 in the Aging-4 simulation and decreased by 26% in the Aging-0.25 simulation, both
605 relative to the Aging-on (base) simulation.

606 Increasing the rate constant by a factor of 4 enhances OPOA concentrations
607 (increase by a factor of 3.3) more than ASOA concentrations (increase by a factor of 2).
608 IVOCs and their aging processes may contribute to the difference in the enhancement
609 between OPOA and ASOA because primary and oxygenated S/IVOCs concentrations in
610 the high volatility (C* of 10^6 – 10^2 μg m^{-3}) are lower in the Aging-4 simulation relative
611 to the Aging-on simulation (not shown).

612 OPOA increases from the Aging-on to the Aging-4 simulation mostly due to
613 the faster aging processes of primary and secondary S/IVOCs. ASOA (BSOA)
614 increases from the Aging-on to the Aging-4 simulation due to the faster aging processes
615 of both anthropogenic OVOCs (biogenic OVOCs) and S/IVOCs. The contribution of
616 S/IVOCs aging processes to ASOA and BSOA increases is about one-third of total
617 increases in ASOA and BSOA concentrations from the Aging-on to the Aging-4
618 simulation (not shown).

619

620 **5.1.3. Interaction of anthropogenic and biogenic sources**

621 The sensitivity simulations shown in Sect. 5.1.3 and 5.2 are summarized in Fig.

622 9. The simulation results with aging processes from biogenic sources only (no aging
623 treatment for S/IVOCs and anthropogenic OVOCs) are shown in Fig. 8a and Table 6
624 (the Aging-bio simulation in Table 4). The contribution of aging processes from
625 anthropogenic sources (AN-aging) can be estimated from the difference in OA
626 concentrations between the Aging-on (base case) and Aging-bio simulations (Fig. 9).
627 As expected, the impact of AN-aging on OPOA and ASOA over the outer domain is
628 very large: AN-aging increases OPOA concentrations from 0.0 to 0.37 μg m^{-3} and
629 ASOA concentrations from 0.038 to 0.33 μg m^{-3} (+780%) (Table 6). AN-aging also
630 moderately enhances POA concentrations (+20%, Table 6).

631 BSOA concentrations are also enhanced considerably (+45%) by AN-aging
632 (Table 6). This is because AN-aging produces large amounts of low-volatile organic
633 vapors and OA from anthropogenic VOCs and S/IVOCs, and these vapors shift the
634 gas-particle partitioning ratio of BSOA to the particulate phase. Therefore, AN-aging
635 is very important for OA formation from both anthropogenic and biogenic sources.

636 These results show that BSOA concentrations are substantially enhanced by
637 OA models that can represent realistic OA concentrations from anthropogenic OA in the
638 atmosphere (the VBS scheme in this study), even if we do not change the treatment of
639 BSOA formation processes in the model. In this study, the importance of this effect
640 was shown for springtime over East Asia, where anthropogenic and biogenic emissions
641 interact closely. Similar interaction is expected over other large emission sources such
642 as the United States and Europe, implying the importance of AN-aging to BSOA
643 concentrations on hemispherical and global scales. Therefore, to obtain more accurate
644 simulations of BSOA, which is considered to be dominant globally, it is important to

use a realistic OA formation scheme for anthropogenic sources.

Figure 8a also shows the simulation results with aging processes from anthropogenic sources only (the Aging-an simulation in Table 4). We can estimate the contribution of aging processes from biogenic sources (BIO-aging) by the difference in OA between the Aging-on (base case) and Aging-an simulations (Fig. 9). BIO-aging slightly influences (less than 4 – 7%) POA, OPOA, and ASOA, whereas it is important for BSOA (increased by 210%). Therefore, the enhancement of anthropogenic OA by aging processes of biogenic VOCs is limited. The difference in the importance of AN-aging and BIO-aging is because anthropogenic sources are dominant over East Asia (Fig. 8b).

5.2. Estimation of controllable OA

We estimate the contribution of OA influenced by anthropogenic emission sources (i.e., controllable OA). Here, we assume that biomass burning emissions are not anthropogenic (not controllable) sources, following the treatment in Carlton et al. (2010). To estimate the contribution of controllable OA over East Asia, we conducted sensitivity simulations with various amounts of anthropogenic emissions ranging from 0% to 200% of base case emissions for both gaseous (CO, NO_x, SO_2, VOCs, and primary S/IVOCs) and aerosol species (POA and BC). Other settings are similar to the base case simulation. Biomass burning, biogenic, and volcanic emissions are not changed in these sensitivity simulations.

Period-averaged POA, OPOA, and ASOA concentrations normalized by those in the base case simulation increase almost linearly with anthropogenic emissions over

668 the outer domain in the sensitivity simulations, except for the range of anthropogenic
669 emissions from 0 to 50%, where the contribution from biomass burning sources are
670 dominant (Fig. 10). In the simulation without anthropogenic emissions, POA, OPOA,
671 and ASOA decrease to 20%, 9%, and 2%, respectively, of the base case simulation.
672 This is because the reduction of anthropogenic VOCs, NO_x, and POA reduces OA
673 concentrations by changing VOC concentrations, their oxidation rates, and the
674 gas-particle partitioning of organic compounds. Controllable OA concentrations can
675 be estimated from the differences in OA between the simulations with (100%) and
676 without (0%) anthropogenic emissions (Fig. 9). The fractions of controllable POA,
677 OPOA, and ASOA are 80%, 91%, and 98%, respectively, in our simulations over all of
678 East Asia.

679 The fractions of POA, OPOA, and ASOA in the simulation without
680 anthropogenic emissions (20%, 9%, and 2% of the base case) are smaller than the
681 fractions expected from emissions, because biomass burning sources account for 30%
682 of POA emissions and 10% of aromatics emissions over the outer domain (Fig. 3c and
683 3d). An important reason for these smaller fractions is the lower OH concentrations
684 (by a factor of 3) and the resulting slower oxidation rates of organic vapors in the
685 simulation without anthropogenic emissions compared with the base case simulation.
686 In fact, the fraction of low-volatile organics (sum of vapors and aerosols) is smaller in
687 the simulation without anthropogenic emissions (not shown).

688 BSOA mass concentrations are positively related to the amounts of
689 anthropogenic emissions, though the relationship is weaker than the relationships for
690 POA, OPOA, and ASOA (green line in Fig. 10). The fraction of controllable BSOA is

691 78% in our estimation; thus a large portion of BSOA is formed through the influence of
692 anthropogenic sources (the enhancement of anthropogenic VOCs, NO_x, and preexisting
693 OA) over East Asia.

694 The period-averaged controllable OA concentrations over the outer domain are
695 1.12 μg m^{-3} and are higher than the sum of POA, OPOA, and ASOA concentrations
696 (0.94 μg m^{-3}). The fraction of controllable OA is 87% (Fig. 11a), suggesting that most
697 of OA is controllable and formed anthropogenically in springtime over all of East Asia.
698 The fraction of controllable OA is more than 90% over most of India and China and its
699 outflow regions and 60 – 80% over Southeast Asia, where BSOA concentrations are
700 high (Fig. 11c), though S/IVOCs emissions and their aging processes have large
701 uncertainties (section 2.3). The fraction of controllable $PM_{2.5}$ is 92% in our estimation,
702 though dust and sea salt from natural sources are not considered in this study.

703 We conducted an additional sensitivity simulation to quantify the importance of
704 the oxidant change (OH concentrations by a factor of 3) when estimating the
705 controllable OA concentrations. In this sensitivity simulation, we excluded the
706 emissions from combustion sources for aerosol species and SOA precursors (primary
707 S/IVOCs, aromatics (ARO1 and ARO2), alkanes (ALK4 and ALK5), and olefins
708 (OLE1 and OLE2)) without changing the emissions of the other gaseous species (CO,
709 NO_x, SO_2, and other VOCs). Period-averaged OH concentrations in this sensitivity
710 simulation were nearly the same as those in the base case simulation (the difference
711 between the two simulations is 7% for OH and 0.3% for HO_2 over East Asia). This
712 sensitivity simulation reduced OA concentrations by 73% and BSOA concentrations by
713 42% over East Asia. These results suggest that the OH change by NO_x and VOCs has

714 a large potential to increase controllable OA amounts over East Asia (from 73% to 87%
715 for total OA and from 42% to 78% for BSOA).

716 Carlton et al. (2010) estimated that more than 50% of BSOA in the eastern
717 United States was controllable. Global modeling studies showed that only 31%
718 (Tsigaridis et al., 2006) and 21% (Hoyle et al., 2009) of the simulated SOA increase
719 from the pre-industrial period to the present was formed directly from anthropogenic
720 VOC, and that the vast majority of the remainder was BSOA enhanced by
721 anthropogenic sources (Hoyle et al., 2011). Spracklen et al. (2011) made top-down
722 estimates of a global SOA budget by using AMS measurements and global model
723 simulations: these estimates suggested that 71% of SOA formed in the atmosphere was
724 controllable. The contribution of controllable OA estimated in this study is greater
725 than previously estimated contributions. The higher contribution of controllable OA in
726 this study is because anthropogenic sources are dominant over East Asia and OA is
727 enhanced considerably by aging processes of organic vapors from anthropogenic
728 sources (Sect. 5.1.3).

729 Carlton and Turpin (2013) suggested that aerosol water produced in
730 anthropogenic aerosols (e.g., SO_4) would enhance biogenic SOA mass concentrations in
731 the eastern U. S. through aqueous-phase chemistry. This process is not considered in
732 our model but could be an important mechanism for enhancing controllable OA
733 concentrations in East Asia because the spatial distributions of SO_4 and OA are
734 generally similar over East Asia.

735 Our estimation of the controllable OA fraction may include large uncertainties
736 because biomass burning emissions are still highly uncertain over East Asia (Matsui et

al., 2013a). The estimation may also be highly sensitive to the simulation periods due to the large seasonal and interannual variations of biomass burning over East Asia (Matsui et al., 2013a). Since biomass burning emissions are highest during February-April over Southeast Asia and during March-May over China (Matsui et al., 2013a), a higher fraction of controllable OA is expected during the other seasons in terms of biomass burning emissions.

Without aging processes, the domain- and period averaged controllable OA is 0.18 μg m^{-3}, and the fraction of controllable OA is 75% (Fig. 11b). The fraction is lower than that in the base case simulation with aging processes. This is because the fraction of OPOA and ASOA, which are mainly formed from anthropogenic sources, is larger in the base case simulation. Both the amounts (from 0.18 to 1.12 μg m^{-3}) and the fraction (from 75% to 87%) of controllable OA are increased by aging processes of organic vapors over East Asia.

6. Summary and conclusions

We simulated OA concentrations over East Asia and its outflow region by using the VBS approach. Model simulations were evaluated via comparisons with the AMS measurements in and around Tokyo (at the Komaba and Kisai sites during the IMPACT-2 campaign in summer 2003 and the IMPACT-L campaign in summer 2004) and over the outflow region in East Asia (at the Fukue and Hedo sites during the A-FORCE campaign in spring 2009).

Model simulations with aging processes of organic vapors (S/IVOCs and OVOCs) reproduced the mass concentrations, temporal variations, and formation

760 efficiency (i.e., SOA/O_3 and OA/SO_4 ratio) of observed OA with reasonable accuracy:
761 the model reproduced SOA concentrations to within 25% during the IMPACT campaign
762 (NMB of -21% and -13% at Komaba and Kisai, respectively), the SOA/O_3 ratio to
763 within 25% at Komaba and Kisai, OA concentrations to within 15% at Fukue and within
764 a factor of 2 at Hedo, and the OA/SO_4 ratio to within 30% at Fukue and Hedo. In
765 contrast, the simulations without the aging processes did not capture these features.
766 The model without the aging processes severely underestimated mass concentrations
767 (by 76 – 88%) and formation efficiencies of OA (by 80 – 90%) at the 4 measurement
768 sites. Thus, the oxidation of organic vapors is essential for realistic OA simulations
769 over East Asia.

770 Concentrations of simulated POA and total SOA (OPOA + ASOA + BSOA)
771 peaked over northern and central China and Southeast Asia, corresponding to large
772 source regions of anthropogenic and biomass burning emissions. Concentrations of
773 ASOA (BSOA) were high over central and northern China (Southeast Asia and southern
774 China). Simulated OA concentrations at an altitude of 1 km over East Asia were
775 highly sensitive to aging processes of organic vapors: relative to the results of
776 simulations without aging, total OA concentrations increased from 0.24 to 1.28 $\mu g\ m^{-3}$
777 (+440%). Aging processes also changed OA chemical composition: in the simulation
778 with the aging processes, the contributions of OPOA and ASOA were 29% and 26%,
779 respectively, of total OA, whereas in the simulation without the aging processes, about
780 70% of total OA was POA.

781 We also examined the importance of the aging processes of organic vapors
782 from anthropogenic (AN-aging) and biogenic sources (BIO-aging). AN-aging was

783 very important for the enhancement of OA formation from both anthropogenic and
784 biogenic sources. AN-aging enhanced BSOA concentrations considerably (+45%),
785 while the enhancement of OPOA and ASOA (SOA from anthropogenic sources) by
786 BIO-aging was very limited (less than 4 – 7%). The difference in the importance of
787 AN-aging and BIO-aging is because anthropogenic sources are dominant over East Asia.
788 These results show that BSOA concentrations are substantially enhanced by OA models
789 that can simulate realistic OA concentrations from anthropogenic sources in the
790 atmosphere, even if we do not change the treatment of BSOA formation processes in the
791 model. Therefore, to obtain more accurate simulations of BSOA, which is considered
792 to be dominant globally, it is important to use a realistic OA formation scheme for
793 anthropogenic sources.

794 The fraction of controllable OA estimated in our simulations was 87%,
795 suggesting that most of the OA was controllable and formed anthropogenically in
796 springtime over all of East Asia. The fractions of controllable POA, OPOA, ASOA,
797 and BSOA were 80%, 91%, 98%, and 78%, respectively, which indicated that a large
798 portion of BSOA was formed through the influence of anthropogenic sources (the
799 enhancement of anthropogenic VOCs, NO_x, and preexisting OA). These fractions
800 were greater than the fraction of anthropogenic emissions (70% of OA emissions and
801 90% of aromatics emissions over East Asia during the simulation periods). An
802 important reason for these higher controllable fractions was higher OH concentration
803 resulting in faster oxidation rates of organic vapors by considering anthropogenic
804 sources. Both the amounts (from 0.18 to 1.12 $\mu g\ m^{-3}$) and the fraction (from 75% to
805 87%) of controllable OA were increased by including aging processes of organic vapors

806 over East Asia.

807 This study is a first step to examine OA concentrations and their spatial
808 distributions and the anthropogenic-biogenic interaction in OA formation over East and
809 Southeast Asia and its outflow regions. Further validations of OA, precursor VOCs,
810 and oxidant species especially over southern China and Southeast Asia, where the
811 contribution of biogenic sources are high, are necessary to understand the behavior of
812 OA and the anthropogenic-biogenic interaction over the Asian region more
813 quantitatively.

814

Acknowledgments.

This work was supported by the Ministry of Education, Culture, Sports, Science, and Technology and the Japan Society for the Promotion of Science (MEXT/JSPS) KAKENHI grant numbers 26740014 and 23221001. This work was also supported by the strategic international cooperative program of the Japan Science and Technology Agency, by the global environment research fund of the Ministry of the Environment, Japan (2A-1101), and by the Alliance for Global Sustainability project of the University of Tokyo. J. D. Fast was supported by the U.S. Department of Energy (DOE) Atmospheric System Research (ASR) program under Contract DE-AC06-76RLO 1830 at PNNL. PNNL is operated for the U.S. DOE by Battelle Memorial Institute. The authors thank Nobuyuki Takegawa at the Research Center for Advanced Science and Technology, University of Tokyo for providing the AMS observation data at the Komaba and Kisai sites during the IMPACT campaign. For a portion of the simulations, we used the supercomputer systems in the University of Tokyo and in Japan Agency for Marine-Earth Science and Technology.

832 **References**

833 Abdul-Razzak, H. and Ghan, S. J.: A parameterization of aerosol activation: 2. Multiple
834 aerosol types, J. Geophys. Res., 105, 6837–6844, doi:10.1029/1999JD901161,
835 2000.
836 Adhikary, B., Carmichael, G. R, Kulkarni, S., Wei, C., Tang, Y., D'Allura, A.,
837 Mena-Carrasco, M., Streets, D. G., Zhang, Q., Pierce, R. B, Al-Saadi, J. A.,
838 Emmons, L. K., Pfister, G. G., Avery, M. A., Barrick, J. D., Blake, D. R., Brune,
839 W. H., Cohen, R. C., Dibb, J. E., Fried, A., Heikes, B. G., Huey, L. G., O'Sullivan,
840 D. W., Sachse, G. W., Shetter, R. E., Singh, H. B., Campos, T. L., Cantrell, C. A.,
841 Flocke, F. M., Dunlea, E. J., Jimenez, J. L., Weinheimer, A. J., Crounse, J. D.,
842 Wennberg, P. O., Schauer, J. J., Stone, E. A., Jaffe, D. A., and Reidmiller, D. R.:
843 A regional scale modeling analysis of aerosol and trace gas distributions over the
844 eastern Pacific during the INTEX-B field campaign, Atmos. Chem. Phys., 10,
845 2091 – 2115, 2010.
846 Ahmadov, R., McKeen, S. A., Robinson, A. L., Bahreini, R., Middlebrook, A. M., de
847 Gouw, J. A., Meagher, J., Hsie, E.-Y., Edgerton, E., Shaw, S., and Trainer, M.: A
848 volatility basis set model for summertime secondary organic aerosols over the
849 eastern United States in 2006, J. Geophys. Res., 117, D06301,
850 doi:10.1029/2011JD016831, 2012.
851 Athanasopoulou, E., Vogel, H., Vogel, B., Tsimpidi, A. P., Pandis, S. N., Knote, C., and
852 Fountoukis, C.: Modeling the meteorological and chemical effects of secondary
853 organic aerosols during an EUCAARI campaign, Atmos. Chem. Phys., 13, 625 –
854 645, 2013.

855 Andersson-Sköld, Y. and Simpson, D.: Secondary organic aerosol formation in northern
856 Europe: A model study, J. Geophys. Res., 106, 7357– 7374,
857 doi:10.1029/2000JD900656, 2001.
858 Bahadur, R., Habib, G., and Russell, L. M.: Climatology of PM2.5 organic carbon
859 concentrations from a review of ground-based atmospheric measurements by
860 evolved gas analysis, Atmos. Environ., 43, 1591 – 1602, 2009.
861 Binkowski, F. S. and Shankar, U.: The regional particulate matte model: 1. Model
862 description and preliminary results, J. Geophys. Res., 100(D12), 26191 – 26209,
863 1995.
864 Bond, T. C., Doherty, S. J., Fahey, D. W., Forster, P. M., Berntsen, T., DeAngelo, B. J.,
865 Flanner, M. G., Ghan, S., Kärcher, B., Koch, D., Kinne, S., Kondo, Y., Quinn, P.
866 K., Sarofim, M. C., Schultz, M. G., Schulz, M., Venkataraman, C., Zhang, H.,
867 Zhang, S., Bellouin, N., Guttikunda, S. K., Hopke, P. K., Jacobson, M. Z., Kaiser,
868 J. W., Klimont, Z., Lohmann, U., Schwarz, J. P., Shindell, D., Storelvmo, T.,
869 Warren, S. G., and Zender, C. S.: Bounding the role of black carbon in the climate
870 system: A scientific assessment, J. Geophys. Res. Atmos., 118, 5380 – 5552,
871 doi:10.1002/jgrd.50171, 2013.
872 Carlton, A. G., Pinder, R. W., Bhave, P. V., and Pouliot, G. A.: To what extent can
873 biogenic SOA be controlled?, Environ. Sci. Technol., 44, 3376 – 3380, 2010.
874 Carlton, A. G. and Turpin, B. J.: Particle partitioning potential of organic compounds is
875 highest in the Eastern US and driven by anthropogenic water, Atmos. Chem. Phys.,
876 13, 10203 – 10214, 2013.
877 Carmichael, G. R., Tang, Y., Kurata, G., Uno, I., Streets, D., Woo, J.-H., Huang, H.,

878 Yienger, J., Lefer, B., Shetter, R., Blake, D., Atlas, E., Fried, A., Apel, E., Eisele,
879 F., Cantrell, C., Avery, M., Barrick, J., Sachse, G., Brune, W., Sandholm, S.,
880 Kondo, Y., Singh, H., Talbot, R., Bandy., A., Thorton, D., Clarke, A., and Heikes,
881 B.: Regional-scale chemical transport modeling in support of the analysis of
882 observations obtained during the TRACE-P experiment, J. Geophys. Res.,
883 108(D21), 8823, doi:10.1029/2002JD003117, 2003.
884 Carter, W. P. L.: Documentation of the SAPRC-99 Chemical Mechanism for VOC
885 Reactivity Assessment, Report to the California Air Resources Board. College of
886 Engineering, Center for Environmental Research and Technology, University of
887 California at Riverside, CA. Contracts 92–329 and 95–308, available at:
888 http://www.cert.ucr.edu/~carter/reactdat.htm, 2000.
889 Chung, S. and Seinfeld, J. H.: Global distribution and climate forcing of carbonaceous
890 aerosols, J. Geophys. Res., 107(D19), 4407, doi:10.1029/2001JD001397, 2002.
891 de Gouw, J. and Jimenez, J. L.: Organic aerosols in the Earth's atmosphere, Environ.
892 Sci. Technol., 43, 7614 – 7618, 2009.
893 Dentener, F., Kinne, S., Bond., T., Boucher, O., Cofala, J., Generoso, S., Ginoux, P.,
894 Gong, S., Hoelzemann, J. J., Ito, A., Marelli, L., Penner, J. E., Putaud, J.-P.,
895 Textor, C., Schulz, M., van der Werf, G. R., and Wilson, J.: Emissions of primary
896 aerosol and precursor gases in the years 2000 and 1750 prescribed data-sets for
897 AeroCom, Atmos. Chem. Phys., 6, 4321 – 4344, 2006.
898 Donahue, N. M., Robinson, A. L., Stanier, C. O., and Pandis, S. N.: Coupled
899 partitioning, dilution, and chemical aging of semivolatile organics, Environ. Sci.
900 Technol., 40, 2635 – 2643, 2006.

Donahue, N. M., Epstein, S. A., Pandis, S. N., and Robinson, A. L.: A two-dimensional volatility basis set: 1. Organic-aerosol mixing thermodynamics, Atmos. Chem. Phys., 11, 3303 – 3318, 2011.

Easter, R. C., Ghan, S. J., Zhang, Y., Saylor, R. D., Chapman, E. G., Laulainen, N. S., Abdul-Razzak, H., Leung, L. R., Bian, X. and Zaveri, R. A.: MIRAGE: Model description and evaluation of aerosols and trace gases, J. Geophys. Res., 109, D20210, doi:10.1029/2004JD004571, 2004.

Ervens, B., Turpin, B. J., and Weber, R. J.: Secondary organic aerosol formation in cloud droplets and aqueous particles (aqSOA): a review of laboratory, field and model studies, Atmos. Chem. Phys., 11, 11069 – 11102, 2011.

Fahey, K. M. and Pandis, S. N.: Optimizing model performance: Variable size resolution in cloud chemistry modeling, Atmos. Environ., 35, 4471– 4478, 2001.

Farina, S. C., Adams, P. J., and Pandis, S. N.: Modeling global secondary organic aerosol formation and processing with the volatility basis set: Implications for anthropogenic secondary organic aerosol, J. Geophys. Res., 115, D09202, doi:10.1029/2009JD013046, 2010.

Fast, J. D., Gustafson Jr., W. I., Easter, R. C., Zaveri, R. A., Barnard, J. C., Chapman, E. G., Grell, G. A., and Peckham, S. E.: Evolution of ozone, particulates, and aerosol direct radiative forcing in the vicinity of Houston using a fully coupled meteorology-chemistry-aerosol model, J. Geophys. Res., 111, D21305, doi:10.1029/2005JD006721, 2006.

Fountoukis, C., Racherla, P. N., Denier van der Gon, H. A. C., Polymeneas, P., Charalampidis, P. E., Pilinis, C., Wiedensohler, A., Dall'Osto, M., O'Dowd, C.,

924 and Pandis, S. N.: Evaluation of a three-dimensional chemical transport model
925 (PMCAMx) in the European domain during the EUCAARI May 2008 campaign,
926 Atmos. Chem. Phys., 11, 10331 – 10347, 2011.
927 George, I. J., Vlasenko, A., Slowik, J. G., Broekhuizen, K., and Abbatt, J. P. D.:
928 Heterogeneous oxidation of saturated organic aerosols by hydroxyl radicals:
929 Uptake kinetics, condensed-phase products, and particle size change, Atmos.
930 Chem. Phys., 7, 4187 – 4201, 2007.
931 George, I. J., Slowik, J., and Abbatt, J. P. D.: Chemical aging of ambient organic
932 aerosol from heterogeneous reaction with hydroxyl radicals, Geophys. Res. Lett.,
933 35, L13811, doi:10.1029/2008GL033884, 2008.
934 Goldstein, A. H. and Galbally, I. E.: Known and unexplored organic constituents in the
935 Earth's atmosphere, Environ. Sci. Technol., 41, 1514 – 1521, 2007.
936 Grell, G. A., Peckham, S. E., Schmitz, R., McKeen, S. A., Frost, G., Skamarock, W. C.,
937 and Eder, B: Fully coupled ''online'' chemistry within the WRF model, Atmos.
938 Environ., 39, 6957 – 6975, 2005.
939 Guenther, A., Karl, T., Harley, P., Wiedinmyer, C., Palmer, P. I., and Geron, C.:
940 Estimates of global terrestrial isoprene emissions using MEGAN (Model of
941 Emissions of Gases and Aerosols from Nature), Atmos. Chem. Phys., 6, 3181 –
942 3210, 2006.
943 Hallquist, M., Wenger, J. C., Baltensperger, U., Rudich, Y., Simpson, D., Claeys, M.,
944 Dommen, J., Donahue, N. M., George, C., Goldstein, A. H., Hamilton, J. F.,
945 Herrmann, H., Hoffmann, T., Iinuma, Y., Jang, M., Jenkin, M. E., Jimenez, J. L.,
946 Kiendler-Scharr, A., Maenhaut, W., McFiggans, G., Mental, F., Monod, A.,

947 Pŕevôt, A. S. H., Seinfeld, J. H., Surratt, J. D., Szmigielski, R., and Wildt, J.: The
948 formation, properties and impact of secondary organic aerosol: current and
949 emerging issues, Atmos. Chem. Phys., 9, 5155 – 5236, 2009.
950 Han, Z., Zhang, R., Wang, Q., Wang, W., Cao, J., and Xu, J.: Regional modeling of
951 organic aerosols over China in summertime, J. Geophys. Res., 113, D11202,
952 doi:10.1029/2007JD009436, 2008.
953 Heald, C. L., Jacob, D. J., Park, R. J., Russell, L. M., Huebert, B. J., Seinfeld, J. H.,
954 Liao, H., and Weber, R. J.: A large organic aerosol source in the free troposphere
955 missing from current models, Geophys. Res. Lett., 32, L18809,
956 doi:10.1029/2005GL023831, 2005.
957 Heald, C. L., Henze, D. K., Horowitz, L. W., Feddema, J., Lamarque, J.-F., Guenther,
958 A., Hess, P. G., Vitt, F., Seinfeld, J. H., Goldstein, A. H., and Fung, I.: Predicted
959 change in global secondary organic aerosol concentrations in response to future
960 climate, emissions, and land use change, J. Geophys. Res., 113, D05211,
961 doi:10.1029/2007JD009092, 2008.
962 Heald, C. L., Ridley, D. A., Kreidenweis, S. M., and Drury, E. E.: Satellite observations
963 cap the atmospheric organic aerosol budget, Geophys. Res. Lett., 37, L24808,
964 doi:10.1029/2010GL045095, 2010.
965 Heald, C. L., Coe, H., Jimenez, J. L., Weber, R. J., Bahreini, R., Middlebrook, A. M.,
966 Russell, L. M., Jolleys, M., Fu, T.-M., Allan, J. D., Bower, K. N., Capes, G.,
967 Crosier, J., Morgan, W. T., Robinson, N. H., Williams, P. I., Cubison, M. J.,
968 DeCarlo, P. F., and Dunlea, E. J.: Exploring the vertical profile of atmospheric
969 organic aerosol: comparing 17 aircraft field campaigns with a global model,

970 Atmos. Chem. Phys., 11, 12673 – 12696, 2011.
971 Herndon, S. C., Onasch, T. B., Wood, E. C., Kroll, J. H., Canagaratna, M. R., Jayne, J.
972 T., Zavala, M. A., Knighton, W. B., Mazzoleni, C., Dubey, M. K., Ulbrich, I. M.,
973 Jimenez, J. L., Seila, R., de Gouw, J. A., de Foy, B., Fast, J., Molina, L. T., Kolb,
974 C. E., and Worsnop, D. R.: Correlation of secondary organic aerosol with odd
975 oxygen in Mexico City, Geophys. Res. Lett., 35, L15804,
976 doi:10.1029/2008GL034058, 2008.
977 Hodzic, A., Jimenez, J. L., Madronich, S., Canagaratna, M. R., DeCarlo, P. F.,
978 Kleinman, L., and Fast, J.: Modeling organic aerosols in a megacity: potential
979 contribution of semi-volatile and intermediate volatility primary organic
980 compounds to secondary organic aerosol formation, Atmos. Chem. Phys., 10,
981 5491 – 5514, 2010.
982 Hoyle, C. R., Myhre, G., Berntsen, T. K., and Isaksen, I. S. A.: Anthropogenic influence
983 on SOA and the resulting radiative forcing, Atmos. Chem. Phys., 9, 2715 – 2728,
984 2009.
985 Hoyle, C. R., Boy. M., Donahue, N. M., Fry, J. L., Glasius, M., Guenther, A., Hallar, A.
986 G., Huff Hartz, K., Petter, M. D., Petäjä, T., Rosenoern, T., and Sullivan, A. P.: A
987 review of the anthropogenic influence on biogenic secondary organic aerosol,
988 Atmos. Phys. Chem., 11, 321 – 343, 2011.
989 Huang, H., Ho, K. F., Lee, S. C., Tsang, P. K., Ho, S. S. H., Zou, C. W., Zou, S. C., Cao,
990 J. J., and Xu, H. M.: Characteristics of carbonaceous aerosol in $PM_{2.5}$: Pearl Delta
991 River Region, China, Atmos. Res., 104-105, 227 – 236, 2012.
992 Iinuma, Y., Böge, O., Gnauk, T. and Herrmann, H.: Aerosol-chamber study of the

993 α-pinene/O_3 reaction: Influence of particle acidity on aerosol yields and products,
994 Atmos. Environ., 38, 761 – 773, 2004.
995 Jacobson, M. Z., Turco, R. P., Jensen, E. J., and Toon, O. B.: Modeling coagulation
996 among particles of different composition and size, Atmos. Environ., 28, 1327–
997 1338, 1994.
998 Jathar, S. H., Farina, S. C., Robinson, A. L., and Adams, P. J.: The influence off
999 semi-volatile and reactive primary emissions on the abundance and properties of
1000 global organic aerosol, Atmos. Chem. Phys., 11, 7727 – 7746, 2011.
1001 Jiang, F., Liu, Q. Huang, X. X., Wang, T. J., Zhuang, B. L., and Xie, M.: Regional
1002 modeling of secondary organic aerosol over China using WRF/Chem, J. Aerosol
1003 Sci., 43, 57 – 73, 2012.
1004 Jimenez, J. L., Canagaratna, M. R., Donahue, N. M., et al.: Evolution of organic
1005 aerosols in the atmosphere, Science, 326, 1525 – 1529, 2009.
1006 Kalberer, M., Paulsen, D., Sax, M., Steinbacher, M., Dommen, J., Prevot, A. S. H.,
1007 Fisseha, R., Weingartner, E., Frankevich, V., Zanobi, R., Baltensperger, U.:
1008 Identification of polymers as major components of atmospheric organic aerosols,
1009 Science, 303, 1659 – 1662, 2004.
1010 Kanakidou, M., Seinfeld, J. H., Pandis, S. N., Barnes, I., Dentener, F. J., Facchini, M. C.,
1011 Van Dingenen, R., Ervens, B., Nenes, A., Nielsen, C. J., Swietlicki, E., Putaud, J.
1012 P., Balkanski, Y., Fuzzi, S., Horth, J., Moortgat, G. K., Winterhalter, R., Myhre, C,
1013 E. L., Tsigaridis, K., Vignati, E., Stephanou, E. G., and Wilson, J.: Organic
1014 aerosol and global climate modeling: A review, Atmos. Chem. Phys., 5, 1053–
1015 1123, 2005.

1016 Kanaya, Y., Cao, R., Akimoto, H., Fukuda, M., Komazaki, Y., Yokouchi, Y., Koike, M.,
1017 Tanimoto, H., Takegawa, N., and Kondo, Y.: Urban photochemistry in central
1018 Tokyo: 1. Observed and modeled OH and HO2 radical concentrations during the
1019 winter and summer of 2004, J. Geophys. Res., 112, D21312,
1020 doi:10.1029/2007JD008670, 2007.
1021 Kannari, A., Baba, T., Ueda, H., Tonooka, Y., and Matsuda, K.: Development of a grid
1022 database on atmospheric pollutants emissions in Japan, (in Japanese), J. Jpn. Soc.
1023 Atmos. Environ., 39(6), 257– 271, 2004.
1024 Kondo, Y., Komazaki, Y., Miyazaki, Y., Moteki, N., Takegawa, N., Kodama, D.,
1025 Deguchi, S., Nogami, M., Fukuda, M., Miyakawa, T., Morino, Y., Koike, M.,
1026 Sakurai, H., and Ehara, K.: Temporal variations of elemental carbon in Tokyo, J.
1027 Geophys. Res., 111, D12205, doi:10.1029/2005JD006257, 2006.
1028 Kondo, Y., Miyazaki, Y., Takegawa, N., Miyakawa, T., Weber, R. J., Jimenez, J. L.,
1029 Zhang, Q., and Worsnop, D. R.: Oxygenated and water-soluble organic aerosols in
1030 Tokyo, J. Geophys. Res., 112, D01203, doi:10.1029/2006JD007056, 2007.
1031 Kondo, Y. Morino, Y., Fukuda, M., Kanaya, Y., Miyazaki, Y., Takegawa, N., Tanimoto,
1032 H., McKenzie, R., Johnston, P., Blake, D. R., Murayama, T., and Koike, M:
1033 Formation and transport of oxidized reactive nitrogen, ozone, and secondary
1034 organic aerosol in Tokyo, J. Geophys. Res., 113, D21310,
1035 doi:10.1029/2008JD010134, 2008.
1036 Kondo, Y., Takegawa, N., Matsui, H., Miyakawa, T., Koike, M., Miyazaki, Y., Kanaya,
1037 Y., Mochida, M., Kuwata, M., Morino, Y., and Shiraiwa, M.: Formation and
1038 transport of aerosols in Tokyo in relation to their physical and chemical properties:

1039 A review, J. Meteor. Soc. Japan, 88, 597 – 624, 2010.
1040 Kondo, Y., Oshima, N., Kajino, M., Mikami, R., Moteki, N., Takegawa, N., Verma, R.
1041 L., Kajii, Y., Kato, S., and Takami, A.: Emissions of black carbon in East Asia
1042 estimated from observations at a remote site in the East China Sea, J. Geophys.
1043 Res., 116, D16201, doi:10.1029/2011JD015637, 2011.
1044 Koo, B., Ansari, A. S., and Pandis, S. N.: Integrated approaches to modeling the organic
1045 and inorganic atmospheric aerosol components, Atmos. Environ., 37, 4757 – 4768,
1046 2003.
1047 Kroll, J. H., Smith, J. D., Che, D. L., Kessler, S. H., Worsnop, D. R., and Wilson, K. R.:
1048 Measurement of fragmentation and functionalization pathways in the
1049 heterogeneous oxidation of oxidized organic aerosol, Phys. Chem. Chem. Phys. 11,
1050 8005 – 8014, 2009.
1051 Lane, T. E., Donahue, N. M., and Pandis, S. N.: Effect of NOx on secondary organic
1052 aerosol concentrations, Environ. Sci. Technol., 42, 6022 – 6027, 2008a.
1053 Lane, T. E., Donahue, N. M., and Pandis, S. N.: Simulating secondary organic aerosol
1054 formation using the volatility basis-set approach in a chemical transport model,
1055 Atmos. Environ., 42, 7439 – 7451, 2008b.
1056 Levine, S. Z. and Schwartz, S. E.: In-cloud and below-cloud scavenging of nitric acid
1057 vapor, Atmos. Environ., 16, 1725 – 1734, 1982.
1058 Li, N., Fu, T.-M., Cao, J., Lee, S., Huang, X.-F., He, L.-Y., Ho, K.-F., Fu, J. S., and
1059 Lam, Y.-F.: Sources of secondary organic aerosols in the Pearl River Delta region
1060 in fall: Contributions from the aqueous reactive uptake of dicarbonyls, Atmos.
1061 Environ., 76, 200 – 207, 2013.

1062 Lim, B., Tan, Y., Perri, M. J., Seitzinger, S. P., and Turpin, B. J.: Aqueous chemistry
1063 and its role in secondary organic aerosol (SOA) formation, Atmos. Chem. Phys.,
1064 10, 10521 – 10539, 2010.
1065 Liu, J., Horowitz, L. W., Fan, S., Carlton, A. G., and Levy II, H.: Global in-cloud
1066 production of secondary organic aerosols: Implementation of a detailed chemical
1067 mechanism in the GFDL atmospheric model AM3, J. Geophys. Res., 117, D15303,
1068 doi:10.1029/2012JD017838, 2012.
1069 Mahmud, A. and Barsanti, K.: Improving the representation of secondary organic
1070 aerosol (SOA) in the MOZART-4 global chemical transport model, Geosci. Model.
1071 Dev., 6, 961 – 980, 2013.
1072 Matsui, H., Koike, M. Takegawa, N. Kondo, Y., Griffin, R. J., Miyazaki, Y., Yokouchi,
1073 Y., and Ohara, T.: Secondary organic aerosol formation in urban air: Temporal
1074 variations and possible contributions from unidentified hydrocarbons, J. Geophys.
1075 Res., 114, D04201, doi:10.1029/2008JD010164, 2009a.
1076 Matsui, H., Koike, M., Kondo, Y., Takegawa, N., Kita, K., Miyazaki, Y., Hu, M.,
1077 Chang, S.-Y., Blake, D. R., Fast, J. D., Zaveri, R. A., Streets, D. G., Zhang, Q.,
1078 and Zhu, T: Spatial and temporal variations of aerosols around Beijing in summer
1079 2006: Model evaluation and source apportionment, J. Geophys. Res., 114,
1080 D00G13, doi:10.1029/2008JD010906, 2009b.
1081 Matsui, H., Koike, M., Kondo, Y., Takegawa, N., Fast, J. D., Pöschl, U., Garland, R. M.,
1082 Andreae, M. O., Wiedensohler, A., Sugimoto, N., and Zhu, T.: Spatial and
1083 temporal variations of aerosols around Beijing in summer 2006: 2. Local and
1084 column aerosol optical properties, J. Geophys. Res., 115, D22207,

doi:10.1029/2010JD013895, 2010.

Matsui, H., Kondo, Y., Moteki, N., Takegawa, N., Sahu, L. K., Zhao, Y., Fuelberg, H. E., Sessions, W. R., Diskin, G., Blake, D. R., Wisthaler, A., and Koike, M.: Seasonal variation of the transport of black carbon aerosol from the Asian continent to the Arctic during the ARCTAS aircraft campaign, J. Geophys. Res., 116, D05202, doi:10.1029/2010JD015067, 2011a.

Matsui, H., Kondo, Y., Moteki, N., Takegawa, N., Sahu, L. K., Koike, M., Zhao, Y., Fuelberg, H. E., Sessions, W. R., Diskin, G., Anderson, B. E., Blake, D. R., Wisthaler, A., Cubison, M. J., and Jimenez, J. L.: Accumulation-mode aerosol number concentrations in the Arctic during the ARCTAS aircraft campaign: Long-range transport of polluted and clean air from the Asian continent, J. Geophys. Res., 116, D20217, doi:10.1029/2011JD016189, 2011b.

Matsui, H., Koike, M., Kondo, Y., Takegawa, N., Wiedensohler, A., Fast, J. D., and Zaveri, R. A.: Impact of new particle formation on the concentrations of aerosols and cloud condensation nuclei around Beijing, J. Geophys. Res., 116, D19208, doi:10.1029/2011JD016025, 2011c.

Matsui, H., Koike, M., Kondo, Y., Oshima, N., Moteki, N., Kanaya, Y., Takami, A., and Irwin, M.: Seasonal variations of Asian black carbon outflow to the Pacific: Contribution from anthropogenic sources in China and biomass burning sources in Siberia and Southeast Asia, J. Geophys. Res. Atmos., 118, 9948–9967, doi:10.1002/jgrd.50702, 2013a.

Matsui, H., Koike, M., Kondo, Y., Moteki, N., Fast, J. D., and Zaveri, R. A.: Development and validation of a black carbon mixing state resolved

three-dimensional model: Aging processes and radiative impact, J. Geophys. Res. Atmos., 118, doi:10.1029/2012JD018446, 2013b.

Matsui, H., Koike, M., Takegawa, N., Kondo, Y., Takami, A., Takamura, T., Yoon, S., Kim, S.-W., Lim, H.-C., and Fast, J. D.: Spatial and temporal variations of new particle formation in East Asia using an NPF-explicit WRF-chem model: North-south contrast in new particle formation frequency, J. Geophys. Res. Atmos., 118, doi:10.1002/jgrd.50821, 2013c.

McKeen, S., Chung, S. H., Wilczak, J., Grell, G., Djalalova, I., Peckham, S., Gong, W., Bouchet, V., Moffet, R., Tang, Y., Carmichael, G. R., Mathur, R., and Yu, S.: Evaluation of several $PM_{2.5}$ forecast models using data collected during the ICARTT/NEAQS 2004 field study, J. Geophys. Res., 112, D10S20, doi:10.1029/2006JD007608, 2007.

Murphy, B. N., Donahue, N. M., Fountoukis, C., and Pandis S. N.: Simulating the oxygen content of ambient organic aerosol with the 2D volatility basis set, Atmos. Chem. Phys. 11, 7859 – 7873, 2011.

Murphy, B. N., Donahue, N. M., Fountoukis, C., Dall'Osto, N., O'Dowd, C., Kiendler-Scharr, A., and Pandis, S. N.: Functionalization and fragmentation during ambient organic aerosol aging: application of the 2-D volatility basis set to field studies, Atmos., Chem., Phys., 12, 10797 – 10816, 2012.

Odum, J. R., Hoffmann, T., Bowman, F., Collins, D., Flagan, R. C., and Seinfeld, J. H.: Gas/particle partitioning and secondary organic aerosol yields, Environ. Sci. Technol., 30, 2580 – 2585, 1996.

Odum, J. R., Jungkamp, T. P. W., Griffin, R. J., Flagan, R. C., and Seinfeld, J. H.: The

1131 atmospheric aerosol-forming potential of whole gasoline vapor, Science, 276, 96 –
1132 99, 1997.
1133 Oshima, N., Kondo, Y., Moteki, N., Takegawa, N., Koike, M., Kita. K., Matsui, H.,
1134 Kajino, M., Nakamura, H., Jung, J. S., and Kim, Y. J.: Wet removal of black
1135 carbon in Asian outflow: Aerosol Radiative Forcing in East Asia (A-FORCE)
1136 aircraft campaign, J. Geophys. Res., 117, D03204, doi:10.1029/2011JD016552,
1137 2012.
1138 Oshima., N., Koike, M., Kondo, Y., Nakamura, H., Moteki, N., Matsui, H., Takegawa,
1139 N., and Kita, K.: Vertical transport mechanisms of black carbon over East Asia in
1140 spring during the A-FORCE aircraft campaign, J. Geophys. Res. Atmos., 118,
1141 13175 – 13198, doi:10.1002/2013JD020262, 2013.
1142 Pye, H. O. T. and Seinfeld, J. H.: A global perspective on aerosol from low-volatility
1143 organic compounds, Atmos. Chem. Phys., 10, 4377 – 4401, 2010.
1144 Ramanathan, V., Crutzen, P. J., Kiehl, J. T., and Rosenfeld, D.: Aerosols, climate, and
1145 the hydrological cycle, Science, 294(5549), 2119–2124, 2001.
1146 Robinson, A. L., Donahue, N. M., Shrivastava, M. K., Weitkamp, E. A., Sage, A. M.,
1147 Grieshop, A. P., Lane, T. E., Pierce, J. R., and Pandis, S. N.: Rethinking organic
1148 aerosols: Semivolatile emissions and photochemical aging, Science, 315, 1259 –
1149 1262, 2007.
1150 Sahu, L. K., Kondo, Y., Miyazaki, Y., Pongkiatkul, P., and Kim Oanh, N. T.: Seasonal
1151 and diurnal variations of black carbon and organic carbon aerosols in Bangkok, J.
1152 Geophys. Res., 116, D15302, doi:10.1029/2010JD015563, 2011.
1153 Schell, B., Ackermann, I. J., Hass, H., Binkowski, F. S., and Ebel, A.: Modeling the

1154 formation of secondary organic aerosol within a comprehensive air quality model
1155 system, J. Geophys. Res., 106, 28275–28293, doi:10.1029/2001JD000384, 2001.
1156 Shirai, T., Yokouchi, Y., Blake, D. R., Kita, K., Izumi, K., Koike, M., Komazaki, Y.,
1157 Miyazaki, Y., Fukuda, M., and Kondo, Y.: Seasonal variations of atmospheric
1158 C2–C7 nonmethane hydrocarbons in Tokyo, J. Geophys. Res., 112, D24305,
1159 doi:10.1029/2006JD008163, 2007.
1160 Shrivastava, M., Fast, J., Easter, R., Gustafson Jr., W. I., Zaveri, R. A., Jimenez, J. L.,
1161 Saide, P., and Hodzic, A.: Modeling organic aerosols in a megacity: comparison
1162 of simple and complex representations of the volatility basis set approach, Atmos.
1163 Chem. Phys., 11, 6639 – 6662, 2011.
1164 Shrivastava, M., Zelenyuk, A., Imre, D., Easter, R., Beranek, J., Zaveri, R. A., and Fast,
1165 J.: Implications of low volatility SOA and gas-phase fragmentation reactions on
1166 SOA loadings and their spatial and temporal evolution in the atmosphere, J.
1167 Geophys. Res. Atmos., 118, 3328–3342, doi:10.1002/jgrd.50160, 2013.
1168 Skamarock, W. C., Klemp, J. B., Dudhia, J., Gill, D. O., Barker, D. M., Wang, W., and
1169 Powers, J. G.: A description of the advanced research WRF version 3, NCAR
1170 Tech. Note, NCAR/TN-475+STR, Natl. Cent. Atmos. Res., Boulder, Colo, 2008.
1171 Spracklen, D. V., Jimenez, J. L., Carslaw, K. S., Worsnop, D. R., Evans, M. J., Mann, G.
1172 W., Zhang, Q., Canagaratna, M. R., Allan, J., Coe, H., McFiggans, G., Rap, A.,
1173 and Forster, P.: Aerosol mass spectrometer constraint on the global secondary
1174 organic aerosol budget, Atmos. Chem. Phys., 11, 12109 – 12136, 2011.
1175 Streets, D. G., Bond, T. C., Carmichael, G. R., Fernandes, S. D., Fu, Q., He, D.,
1176 Klimont, Z., Nelson, S. M., Tsai, N. Y., Wang, M. Q., Woo, J.-H., and Yarber, K.

1177 F.: An inventory of gaseous and primary aerosol emissions in Asia in the year
1178 2000, J. Geophys. Res., 108(D21), 8809, doi:10.1029/2002JD003093, 2003.
1179 Takami, A., Miyoshi, T., Shimono, A., and Hatakeyama, S.: Chemical composition of
1180 fine aerosol measured by AMS at Fukue Island, Japan, during APEX period,
1181 Atmos. Environ., 39, 4913–4924, 2005.
1182 Takami, A., Miyoshi, T., Shimono, A., Kaneyasu, N., Kato, S., Kajii, Y., and
1183 Hatakeyama, S.: Transport of anthropogenic aerosols from Asia and subsequent
1184 chemical transformation, J. Geophys. Res., 112, D22S31,
1185 doi:10.1029/2006JD008120, 2007.
1186 Takegawa, N., Miyazaki, Y., Kondo, Y., Komazaki, Y., Miyakawa, T., Jimenez, J. L.,
1187 Jayne, J. T., Worsnop, D. R., Allan, J., and Weber, R. J.: Characterization of an
1188 Aerodyne aerosol mass spectrometer (AMS): Intercomparison with other aerosol
1189 instruments, Aerosol Sci. Technol., 39, 760–770, 2005.
1190 Takegawa, N., T. Miyakawa, Kondo, Y., Blake, D. R., Kanaya, Y., Koike, M., Fukuda,
1191 M., Komazaki, Y., Miyazaki, Y., Shimono, A., and Takeuchi, T.: Evolution of
1192 submicron organic aerosol in polluted air exported from Tokyo, Geophys. Res.
1193 Lett., 33, L15814, doi:10.1029/2006GL025815, 2006a.
1194 Takegawa, N., Miyakawa, T., Kondo, Y., Jimenez, J. L., Zhang, Q., Worsnop, D. R.,
1195 and Fukuda, M.: Seasonal and diurnal variations of submicron organic aerosols in
1196 Tokyo observed using the Aerodyne aerosol mass spectrometer, J. Geophys. Res.,
1197 111, D11206, doi:10.1029/2005JD006515, 2006b.
1198 Tao, J., Shen, Z. Zhu, C., Yue, J., Cao, J., Liu, S., Zhu, L., and Zhang, R.: Seasonal
1199 variations and chemical characteristics of sub-micrometer particles (PM_1) in

Guangzhou, China, Atmos. Res., 118, 222 – 231, 2012.

Tsigaridis, K. and Kanakidou, M.: Global modelling of secondary organic aerosol in the troposphere: a sensitivity analysis, Atmos. Chem. Phys., 3, 1849 – 1869, 2003.

Tsigaridis, K. and Kanakidou, M.: Secondary organic aerosol importance in the future atmosphere, Atmos. Environ., 41, 4682–4692, 2007.

Tsigaridis, K., Krol, M., Dentener, F. J., Balkanski, Y., Lathiere, J., Metzger, S., Hauglustaine, D. A., and Kanakidou, M.: Change in global aerosol composition since preindustrial times, Atmos. Chem. Phys., 6, 5143 – 5162, 2006.

Tsimpidi, A. P., Karydis, V. A., Zavala, M., Lei, W., Molina, L., Ulbrich, I. M., Jimenez, J. L., and Pandis, S. N.: Evaluation of the volatility basis-set approach for the simulation of organic aerosol formation in the Mexico City metropolitan area, Atmos. Chem. Phys., 10, 525 – 546, 2010.

Tsimpidi, A. P., Karydis, V. A., Zavala, M., Lei, W., Bei, N., Molina, L., and Pandis S. N.: Sources and production of organic aerosol in Mexico City: insights from the combination of a chemical transport model (PMCAMx-2008) and measurements during MILAGRO, Atmos. Chem. Phys., 11, 5153 – 5168, 2011.

Turpin, B. J. and Lim, H. J.: Species contributions to $PM_{2.5}$ mass concentrations: Revisiting common assumptions for estimating organic mass, Aerosol Sci. Technol., 35, 602– 610, 2001.

Utembe, S. R., Cooke, M. C., Archibald, A. T., Shallcross, D. E., Derwent, R. G., and Jenkin, M. E.: Simulating secondary organic aerosol in a 3-D Lagrangian chemistry transport model using the reduced Common Representative Intermediates mechanism (CRI v2-R5), Atmos. Environ., 45, 1604 – 1614, 2011.

van der Werf, G. R., Randerson, J. T., Giglio, L., Collatz, G. J., Mu, M., Kasibhatla, P. S., Morton, D. C., DeFries, R. S., Jin, Y., and van Leeuwen, T. T.: Global fire emissions and the contribution of deforestation, savanna, forest, agricultural, and peat fires (1997 – 2009), Atmos. Chem. Phys., 10, 11707 – 11735, 2010.

Wesely, M. L.: Parameterization of surface resistances to gaseous dry deposition in regional-scale numerical models, Atmos. Environ, 23, 1293–1304, 1989.

Wexler, A. S., Lurmann, F. W., and Seinfeld, J. H.: Modelling urban and regional aerosols. Part I: Model development, Atmos. Environ., 28, 531–546, 1994.

Xiao, R. Takegawa, N., Zheng, M., Kondo, Y., Miyazaki, Y., Miyakawa, T., Hu, M., Shao, M., Zeng, L., Gong, Y., Lu, K., Deng, Z., Zhao, Y., and Zhang, Y. H.: Characterization and source apportionment of submicron aerosol with aerosol mass spectrometer during the PRIDE-PRD 2006 campaign, Atmos. Chem. Phys., 11, 6911 – 6929, 2011.

Zaveri, R. A. and Peters, L. K.: A new lumped structure photochemical mechanism for large-scale applications, J. Geophys. Res., 104, 30,387– 30,415, doi:10.1029/1999JD900876, 1999.

Zaveri, R. A., Easter, R. C., and Wexler, A. S.: A new method for multicomponent activity coefficients of electrolytes in aqueous atmospheric aerosols, J. Geophys. Res., 110, D02201, doi:10.1029/2004JD004681, 2005a.

Zaveri, R. A., Easter, R. C., and Peters, L. K.: A computationally efficient Multicomponent Equilibrium Solver for Aerosols (MESA), J. Geophys. Res., 110, D24203, doi:10.1029/2004JD005618, 2005b.

Zaveri, R. A., Easter, R. C., Fast, J. D., and Peters, L. K.: Model for Simulating Aerosol

1246 Interactions and Chemistry (MOSAIC), J. Geophys. Res., 113, D13204,
1247 doi:10.1029/2007JD008782, 2008.
1248 Zhang, Q., Alfarra, M. R., Worsnop, D. R., Allan, J. D., Coe, H., Canagaratna, M. R.,
1249 and Jimenez, J. L.: Deconvolution and quantification of hydrocarbon-like and
1250 oxygenated organic aerosols based on aerosol mass spectrometry, Environ. Sci.
1251 Technol., 39, 4938–4952, 2005.
1252 Zhang, Q., Jimenez, J. L., Canagaratna, M. R. et al.: Ubiquity and dominance of
1253 oxygenated species in organic aerosols in anthropogenically influenced Northern
1254 Hemisphere midlatitudes, Geophys. Res. Lett., 34, L13801,
1255 doi:10.1029/2007GL029979, 2007.
1256 Zhang, Y., Pun, B., Vijayaraghavan, K., Wu, S.-Y., Seigneur, C., Pandis, S. N.,
1257 Jacobson, M. Z., Nenes, A., and Seinfeld, J. H.: Development and application of
1258 the Model of Aerosol Dynamics, Reaction, Ionization, and Dissolution
1259 (MADRID), J. Geophys. Res., 109, D01202, doi:10.1029/2003JD003501, 2004.
1260
1261

1262 **Author's addresses**

1263 J. D. Fast, Atmospheric Science and Global Change Division, Pacific Northwest
1264 National Laboratory, MSINK9-30, P.O. Box 999, Richland, WA 99352, USA.
1265 (jerome.fast@pnnl.gov)
1266 Y. Kanaya, H. Matsui, and M. Takigawa, Research Institute for Global Change, Japan
1267 Agency for Marine-Earth Science and Technology, 3173-25, Showa-machi,
1268 Kanazawa-ku, Yokohama, Kanagawa, 236-0001, Japan. (yugo@jamstec.go.jp,
1269 matsui@jamstec.go.jp, takigawa@jamstec.go.jp)
1270 M. Koike and Y. Kondo, Department of Earth and Planetary Science, Graduate School
1271 of Science, The University of Tokyo, Hongo 7-3-1, Bunkyo-ku, Tokyo, 113-0033,
1272 Japan. (koike@eps.s.u-tokyo.ac.jp, kondo@eps.s.u-tokyo.ac.jp)
1273 A. Takami, National Institute for Environmental Studies, Onogawa 16-2, Tsukuba,
1274 Ibaraki 305-8506, Japan. (takamia@nies.go.jp)

1275

1276

Figure Captions

Fig. 1. Summary of the volatility basis-set approach used in this study. Circles and squares show individual gas-phase (open) and aerosol-phase (closed) surrogate species. Squares denote primary emission species. AN, BB, and BIO denote anthropogenic, biomass burning, and biogenic sources, respectively. The oxidation processes shown by the black arrows are calculated using the coefficients given by Tsimipidi et al. (2010). The oxidation processes shown by the orange arrows are calculated by assuming OH oxidation with a rate coefficient of 1×10^{-11} cm^{-3} $molecule^{-1}$ s^{-1}.

Fig. 2. Simulation domains (a) in and around Tokyo during the IMPACT campaign and (b) over East Asia during the A-FORCE campaign. (a) Simulations were conducted for 17 July to 15 August 2003 (IMPACT-2) and for 23 July to 15 August 2004 (IMPACT-L) with horizontal resolutions of 27 km (outer domain, orange) and 9 km (inner domain, red). Light blue squares show the locations of the measurement stations at Komaba (35.66°N, 139.67°E) and Kisai (36.08°N, 139.55°E). (b) Simulations were conducted for 21 March to 26 April 2009 with horizontal resolutions of 180 km (outer domain, orange) and 60 km (inner domain, red). Light blue squares show the locations of the measurement stations at Fukue (32.75°N, 128.68°E) and Kisai (26.87°N, 128.25°E).

Fig. 3. Period-averaged (24 March – 26 April 2009) emissions for (a) POA from anthropogenic sources (fossil fuel and biofuel combustion), (b) POA from biomass burning sources, (c) ARO1 (aromatics), and (d) TERP (monoterpenes).

We used the anthropogenic and volcanic emission inventories of Streets et al. (2003), daily biomass burning emissions of the Global Fire Emissions Database version 3 (GFED3) (van der Werf et al., 2010), and on-line biogenic emissions of the Model of Emissions of Gases and Aerosols from Nature version 2 (MEGAN2) (Guenther et al., 2006).

Fig. 4. Time series of the observed and simulated (a) O_3 volume mixing ratios and (b) SOA mass concentrations at Kisai during the IMPACT-L campaign. SOA values were simulated with and without aging.

Fig. 5. Correlation of SOA mass concentrations with O_3 volume mixing ratios (a) at Komaba during the IMPACT-2 campaign and (b) at Kisai during the IMPACT-L campaign. Solid lines show the fitting slopes (y = ax) for observation (blue) and simulations with (red) and without (orange) aging processes of organic vapors.

Fig. 6. Time series of (a, b) black carbon mass concentrations, (c, d) sulfate mass concentrations, (e, f) organic aerosol mass concentrations, and (g, h) organic to sulfate mass concentration ratios at Fukue and Hedo, respectively. Red shading in panels e and f shows the range of organic aerosol mass concentrations with the aging coefficients of between 4×10^{-11} cm^3 $molecule^{-1}$ s^{-1} (4 times the base case) and 2.5×10^{-12} cm^3 $molecule^{-1}$ s^{-1} (1/4 times the base case). The periods when observed sulfate mass concentrations were less than 1 μg m^{-3} are not shown for measurements (blue points) in panels g and h.

Fig. 7. Period-averaged (24 March – 26 April 2009) simulated mass concentrations of POA (a, b), OPOA (c, d), ASOA (e, f), BSOA (g, h), and total SOA (sum of

1323 OPOA, ASOA, and BSOA) (i, j) at an altitude of about 1 km (layer number of
1324 8, sigma level of 0.895). Left panels (a, c, e, g, i) are runs with aging, and
1325 right panels (b, d, f, h, j) are runs without aging.
1326 Fig. 8. Period-averaged (24 March – 26 April 2009) mass concentrations of POA,
1327 OPOA, ASOA, and BSOA at an altitude of about 1 km over the outer domain
1328 for Aging-on, Aging-off, Aging-bio, and Aging-an simulations (a).
1329 Period-averaged fraction of POA, OPOA, ASOA, and BSOA to total OA mass
1330 concentrations at an altitude of about 1 km over the outer domain for
1331 simulations with (b) or without (c) aging.
1332 Fig. 9. Diagram of sensitivity simulations conducted in Sect. 5. OA contributions
1333 estimated from individual simulations are shown. AVOC and BVOC denote
1334 anthropogenic and biogenic OVOCs, respectively.
1335 Fig. 10. Sensitivity of POA, OPOA, ASOA, and BSOA mass concentrations to
1336 changes in anthropogenic emissions (CO, NO_x, SO_2, VOCs, S/IVOCs, POA
1337 and BC) at an altitude of about 1 km over the outer domain. Mass
1338 concentrations and anthropogenic emissions in the sensitivity simulations are
1339 normalized by those in the base case simulation.
1340 Fig. 11. Period-averaged (24 March – 26 April 2009) fraction of controllable and
1341 non-controllable OA mass concentrations at an altitude of about 1 km over the
1342 outer domain for simulations with (a) or without (b) aging. Period-averaged
1343 (24 March – 26 April 2009) fraction of controllable OA at an altitude of about 1
1344 km over the outer domain for the simulation with aging (c).
1345

Table 1. Abbreviations for organic vapors and aerosols used in this study

Abbreviation	Definition	Explanation
OA	Organic aerosol	---
POA	Primary OA	Primary emission or formed from S/IVOCs by equilibrium (w/o oxidation)
SOA	Secondary OA	Sum of OPOA, BSOA, and ASOA
VOCs	Volatile organic compounds	Primary emission
S/IVOCs	Semi-volatile and intermediate volatility organic compounds	Primary emission (primary S/IVOCs) or secondary production through the oxidation of primary S/IVOCs (oxygenated S/IVOCs)
OVOCs	Oxygenated volatile organic compounds	Oxidation products of VOCs
HOA	Hydrocarbon-like OA	Obtained by AMS
OOA	Oxygenated OA	Obtained by AMS
OPOA	Oxygenated POA	OA formed from oxygenated S/IVOCs
BSOA	Biogenic SOA	OA formed from biogenic OVOCs
ASOA	Anthropogenic SOA	OA formed from anthropogenic OVOCs (including biomass burning sources)

Table 2. Meteorological and chemical process options used in this study

Atmospheric Process	Model Option
Longwave radiation	RRTM
Shortwave radiation	Goddard
Surface layer	Monin-Obukhov
Land surface	Noah
Boundary layer	YSU
Cumulus clouds	Kain-Fritsch
Cloud microphysics	Morrison
Gas-phase chemistry	SAPRC99
Aerosol nucleation	Binary nucleation
Aerosol condensation	MOSAIC
Aerosol coagulation	COAGSOLV
Aqueous-phase chemistry	Fahey and Pandis
Photolysis	Fast-J

Table 3. Summary of the VBS schemes developed in this study and original WRF-chem/MOSAIC model

Item/Process	This Study	Shrivastava et al. (2011)
Gas-phase chemistry	SAPRC99	SAPRC99
VBS volatility species	9 for POA and primary S/IVOCs 8 for OPOA and oxygenated S/IVOCs 4 for ASOA, BSOA, and OVOCs	9 for POA and primary S/IVOCs 8 for OPOA and oxygenated S/IVOCs 4 for ASOA, BSOA, and OVOCs
Oxidation species	VOCs, S/IVOCs, and OVOCs	VOCs and S/IVOCs
OVOCs formation	NO_x-dependent 4-product fit (Tsimpidi et al., 2010)	NO_x-dependent 4-product fit (Tsimpidi et al., 2010)
Gas-particle partitioning	Bulk equilibrium (Schell et al., 2001)	Bulk equilibrium (Donahue et al., 2006)
OA distribution to each size bin	Koo et al. (2003)	Koo et al. (2003)
Number of size bin	8 (40 – 10000 nm)	4 (40 – 10000 nm)
Number of variables in VBS	122 Gas-phase: 53 Bulk aerosol: 53 Size-resolved aerosol: 16 (interstitial aerosol, in-cloud aerosol)	380 Gas-phase: 76 Size-resolved aerosol: 304
Dry deposition	On	On
Aerosol activation	On	Off
Wet deposition	On	Off

Table 4. List of model simulations

Simulation	Aging coefficient (cm^3 $molucule^{-1}$ s^{-1})	
	S/IVOCs and anthropogenic OVOCs	Biogenic OVOCs
Aging-on	1e-11	1e-11
Aging-off	0	0
Aging-an	1e-11	0
Aging-bio	0	1e-11
Aging-0.25	2.5e-12	2.5e-12
Aging-4	4e-11	4e-11

Table 5. Statistics of concentrations of chemical species at the surface measurement sites

Station	Period	Species	Units	Mean concentration			NMB (%) [b]	R [b]
				Observation	Calculation [a] (Aging-on)	Calculation [a] (Aging-off)		
Komaba	19 July – 13 August 2003 (IMPACT-2)	O_3	ppbv	19.6	15.3	15.4	-22.3	0.63
		SOA	$\mu g\ m^{-3}$	4.36	3.45	1.03	-20.8	0.52
Kisai	25 July – 14 August 2004 (IMPACT-L)	O_3	ppbv	26.4	20.6	20.7	-21.9	0.84
		SOA	$\mu g\ m^{-3}$	5.31	4.61	0.76	-13.1	0.70
Fukue	27 March – 26 April 2009	BC	$\mu g\ m^{-3}$	0.87	0.75	0.74	-14.2	0.76
		SO_4	$\mu g\ m^{-3}$	9.31	8.29	8.27	-10.9	0.65
		OA	$\mu g\ m^{-3}$	6.02	6.75	0.71	12.2	0.34
		OA/SO_4	---	0.89	0.78	0.13	-11.9	0.28
Hedo	24 March – 26 April 2009	BC	$\mu g\ m^{-3}$	0.36	0.27	0.27	-24.3	0.46
		SO_4	$\mu g\ m^{-3}$	2.36	4.20	4.24	78.0	0.34
		OA	$\mu g\ m^{-3}$	1.08	1.99	0.18	84.2	0.25
		OA/SO_4	---	0.58	0.42	0.058	-29.7	0.58

[a] Values are calculated for the periods when measurements are available.

[b] Statistics are calculated for the Aging-on simulation.

Table 6. Period-averaged organic aerosol mass concentration (μg m^{-3}) in the boundary layer (~ 1 km) over the outer domain

Simulation	POA	OPOA	ASOA	BSOA	Total OA
Aging-on	0.236	0.369	0.333	0.346	1.284
Aging-off	0.164	0.000	0.023	0.048	0.236
Aging-an	0.229	0.357	0.313	0.111	1.004
Aging-bio	0.196	0.000	0.038	0.241	0.474
Aging-0.25	0.188	0.056	0.106	0.132	0.483
Aging-4	0.275	1.223	0.661	0.654	2.813
Aging-on (an off) [a]	0.047	0.035	0.007	0.075	0.165
Aging-off (an off) [a]	0.040	0.000	0.001	0.018	0.059

[a] Simulations without anthropogenic emissions (with biomass burning, biogenic, and volcanic emissions).

Fig. 1

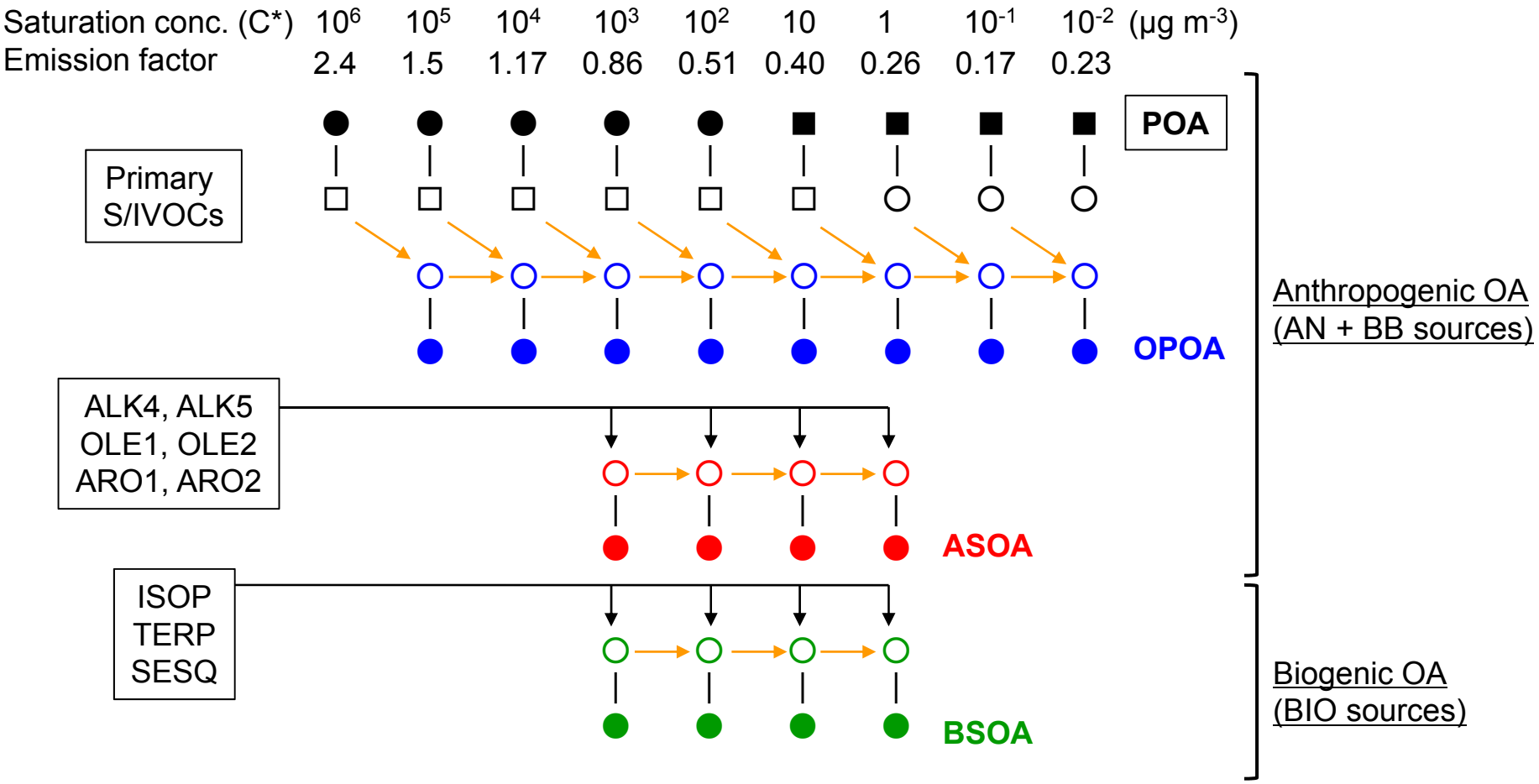
Saturation conc. (C*) 10^6 10^5 10^4 10^3 10^2 10 1 10^-1 10^-2 (μg m^-3)
Emission factor 2.4 1.5 1.17 0.86 0.51 0.40 0.26 0.17 0.23
POA
Primary S/IVOCs
OPOA
ALK4, ALK5 OLE1, OLE2 ARO1, ARO2
ASOA
ISOP TERP SESQ
BSOA
Anthropogenic OA (AN + BB sources)
Biogenic OA (BIO sources)

Fig. 2

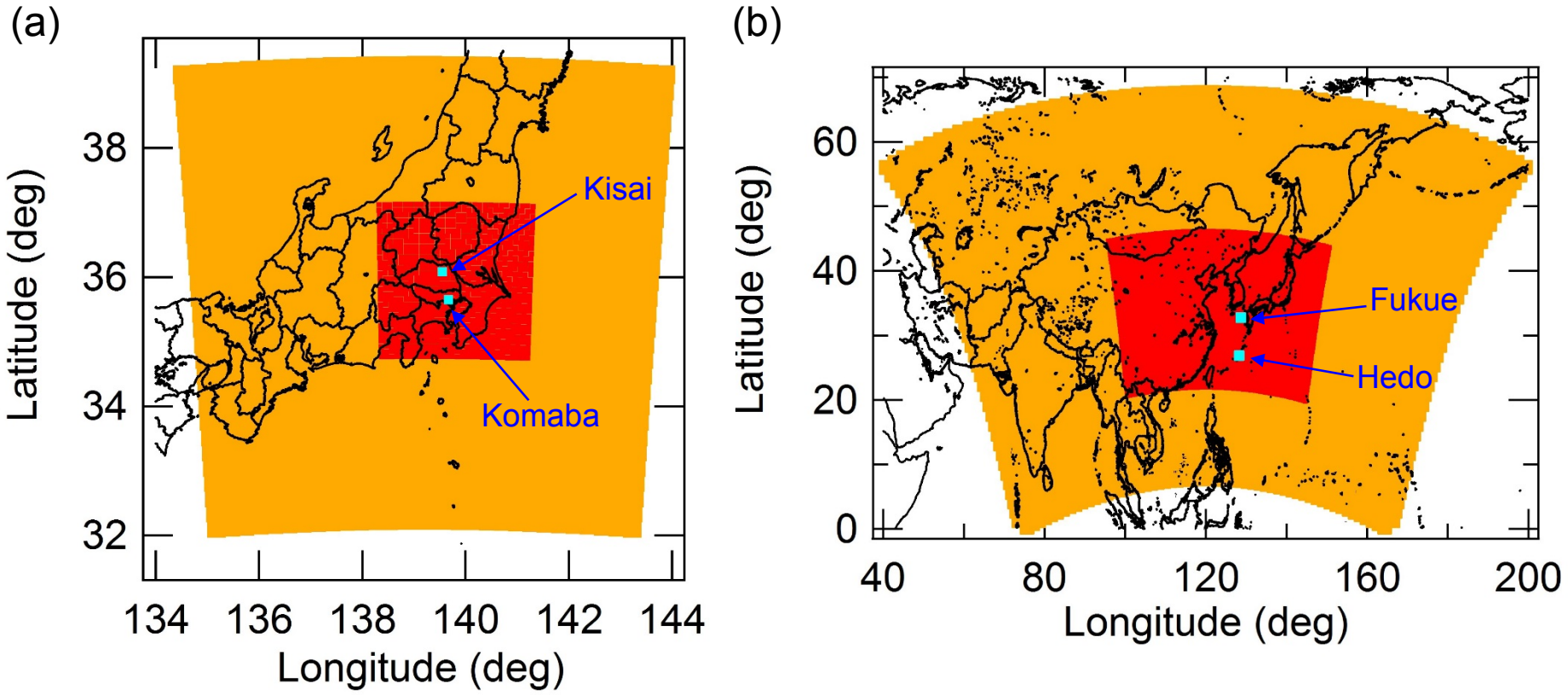
(a)
Kisai
Komaba
38
36
34
32
134
136
138
140
142
144
Latitude (deg)
Longitude (deg)
(b)
Fukue
Hedo
60
40
20
0
40
80
120
160
200
Latitude (deg)
Longitude (deg)

Fig. 3

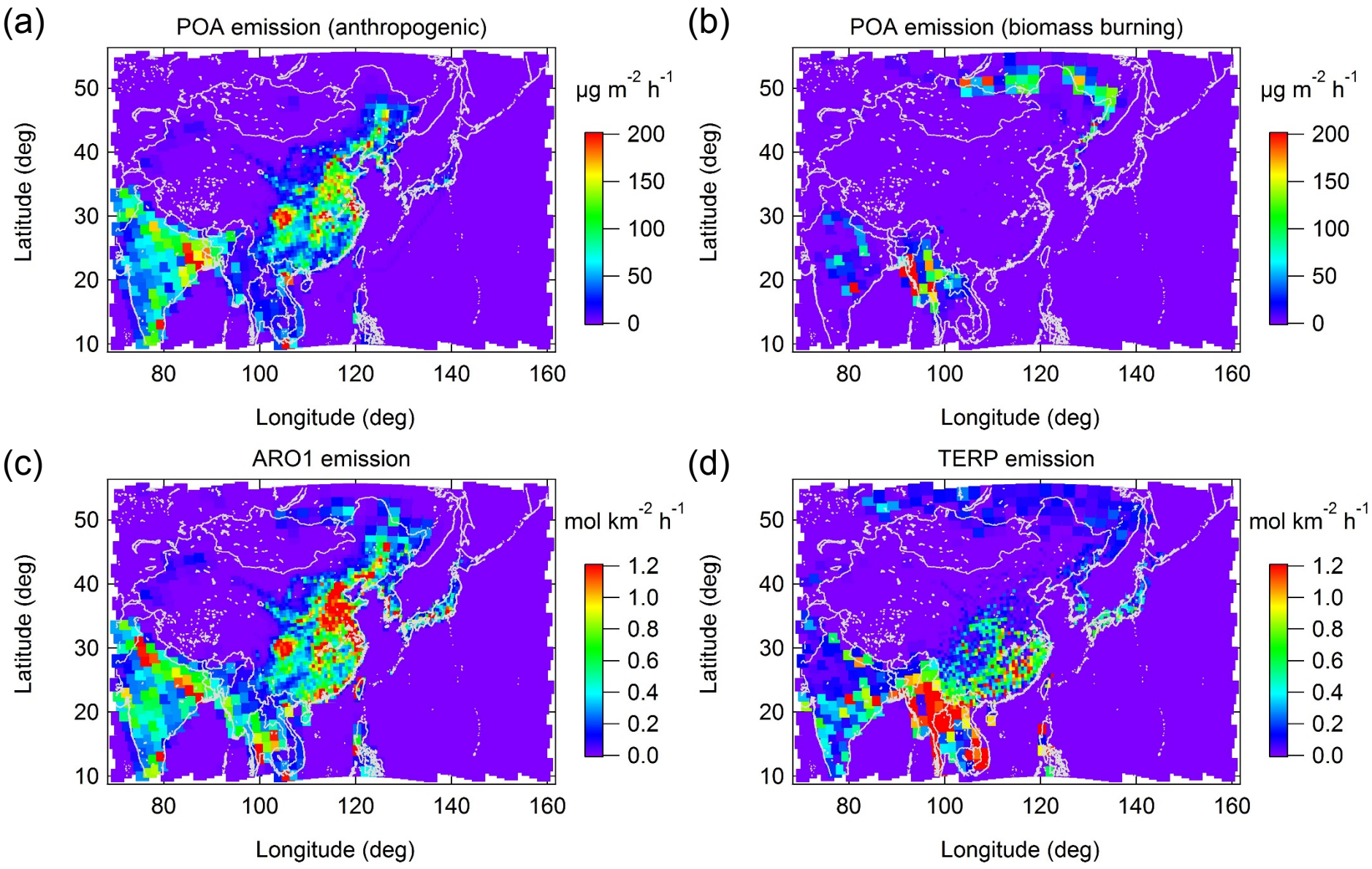
(a)
POA emission (anthropogenic)
μg m-2 h-1
200
150
100
50
0
Latitude (deg)
Longitude (deg)
10
20
30
40
50
80
100
120
140
160
(b)
POA emission (biomass burning)
μg m-2 h-1
200
150
100
50
0
Latitude (deg)
Longitude (deg)
(c)
ARO1 emission
mol km-2 h-1
1.2
1.0
0.8
0.6
0.4
0.2
0.0
Latitude (deg)
Longitude (deg)
(d)
TERP emission
mol km-2 h-1
1.2
1.0
0.8
0.6
0.4
0.2
0.0
Latitude (deg)
Longitude (deg)

Fig. 4

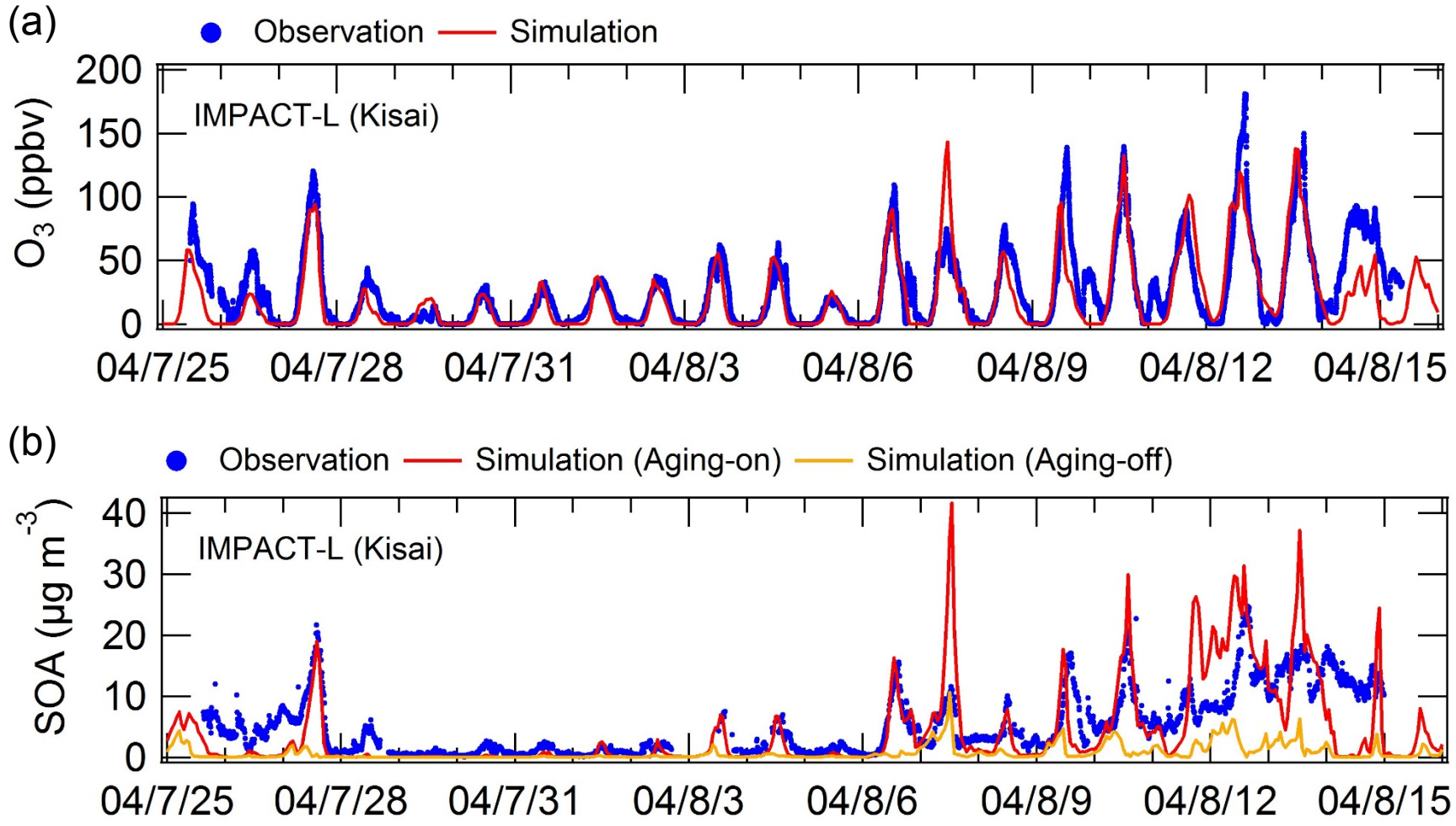
(a)
Observation
Simulation
IMPACT-L (Kisai)
O_3 (ppbv)
200
150
100
50
0
04/7/25
04/7/28
04/7/31
04/8/3
04/8/6
04/8/9
04/8/12
04/8/15
(b)
Observation
Simulation (Aging-on)
Simulation (Aging-off)
IMPACT-L (Kisai)
SOA (μg m^{-3})
40
30
20
10
0
04/7/25
04/7/28
04/7/31
04/8/3
04/8/6
04/8/9
04/8/12
04/8/15

Fig. 5

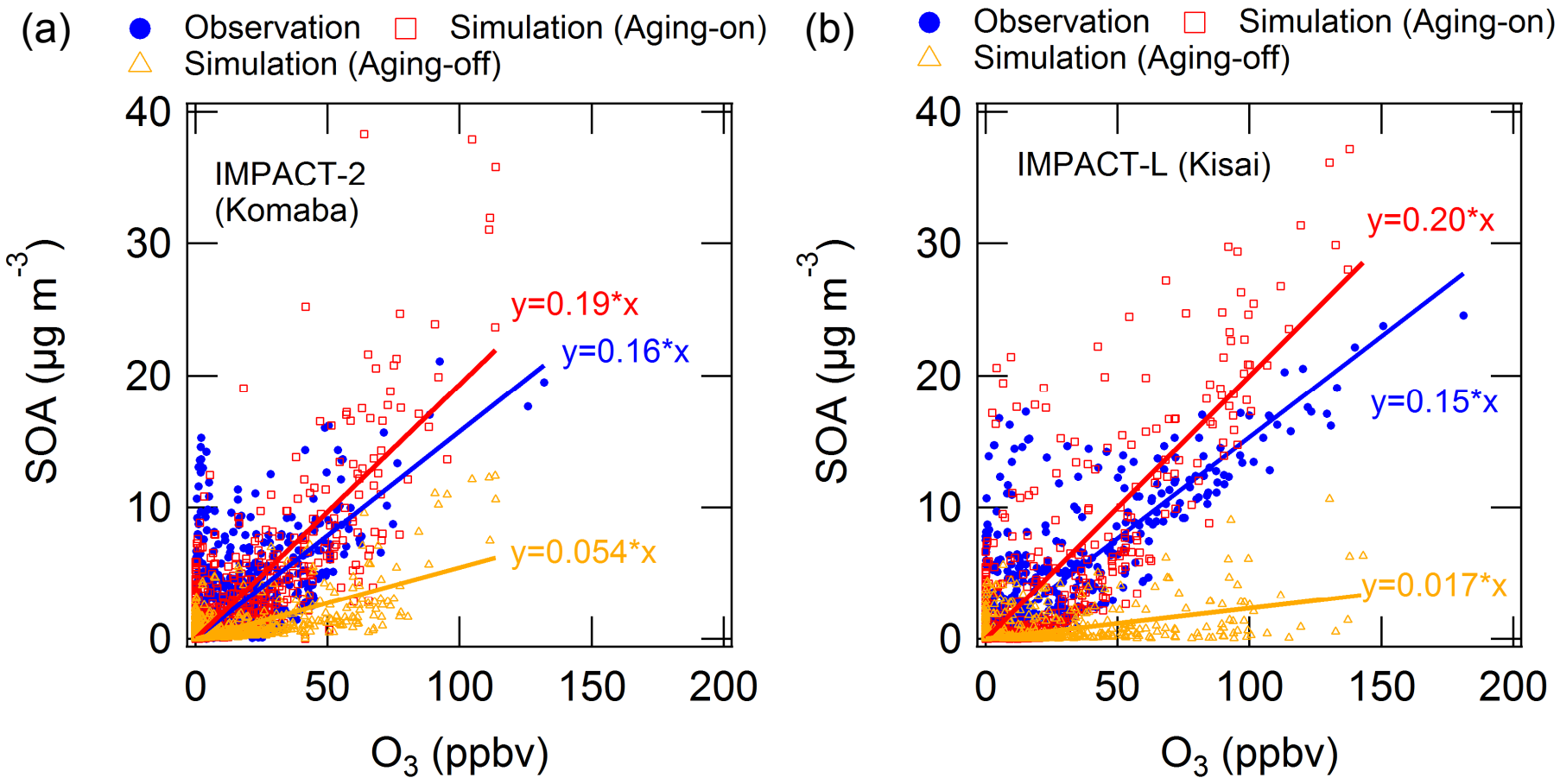
(a)
Observation
Simulation (Aging-on)
Simulation (Aging-off)
IMPACT-2
(Komaba)
y=0.19*x
y=0.16*x
y=0.054*x
SOA (μg m-3)
O3 (ppbv)
0
10
20
30
40
0
50
100
150
200
(b)
Observation
Simulation (Aging-on)
Simulation (Aging-off)
IMPACT-L (Kisai)
y=0.20*x
y=0.15*x
y=0.017*x
SOA (μg m-3)
O3 (ppbv)

Fig. 6

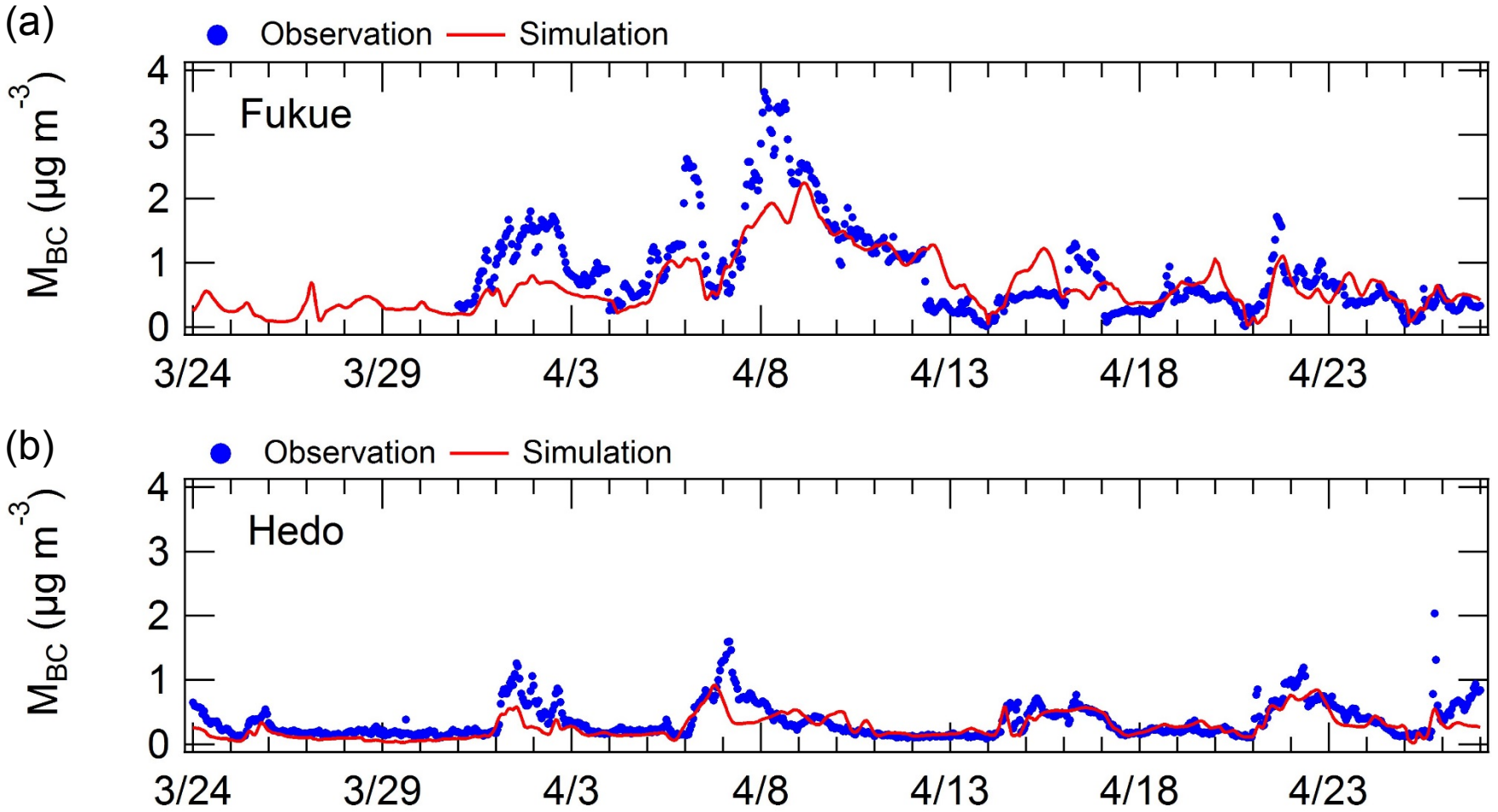
(a)
Observation
Simulation
Fukue
M_{BC} ($\mu g\ m^{-3}$)
0
1
2
3
4
3/24
3/29
4/3
4/8
4/13
4/18
4/23
(b)
Observation
Simulation
Hedo
M_{BC} ($\mu g\ m^{-3}$)
0
1
2
3
4
3/24
3/29
4/3
4/8
4/13
4/18
4/23

Fig. 6 (cont.)

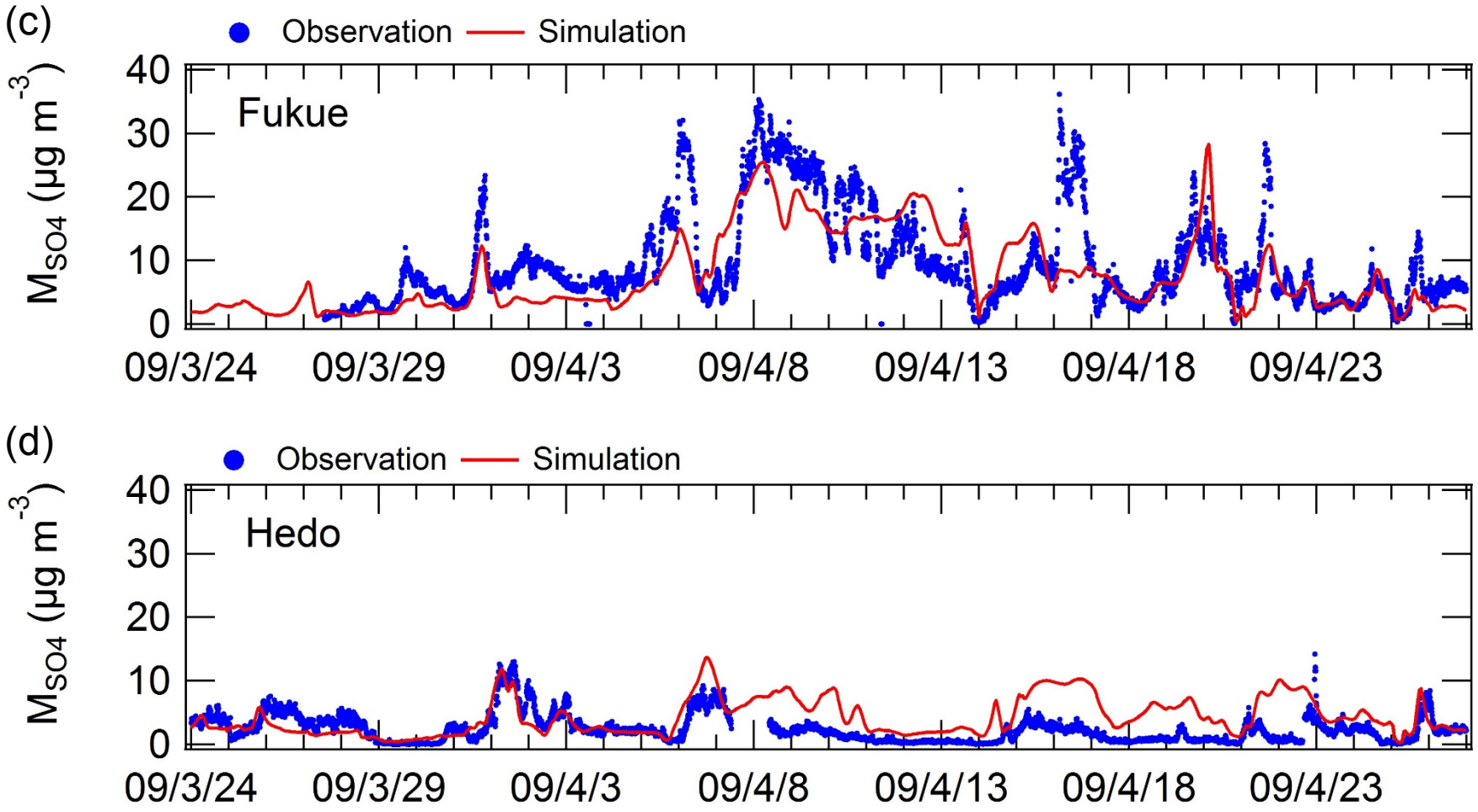
(c)
Observation
Simulation
Fukue
M_{SO4} (μg m^{-3})
40
30
20
10
0
09/3/24
09/3/29
09/4/3
09/4/8
09/4/13
09/4/18
09/4/23
(d)
Observation
Simulation
Hedo
M_{SO4} (μg m^{-3})
40
30
20
10
0
09/3/24
09/3/29
09/4/3
09/4/8
09/4/13
09/4/18
09/4/23

Fig. 6 (cont.)

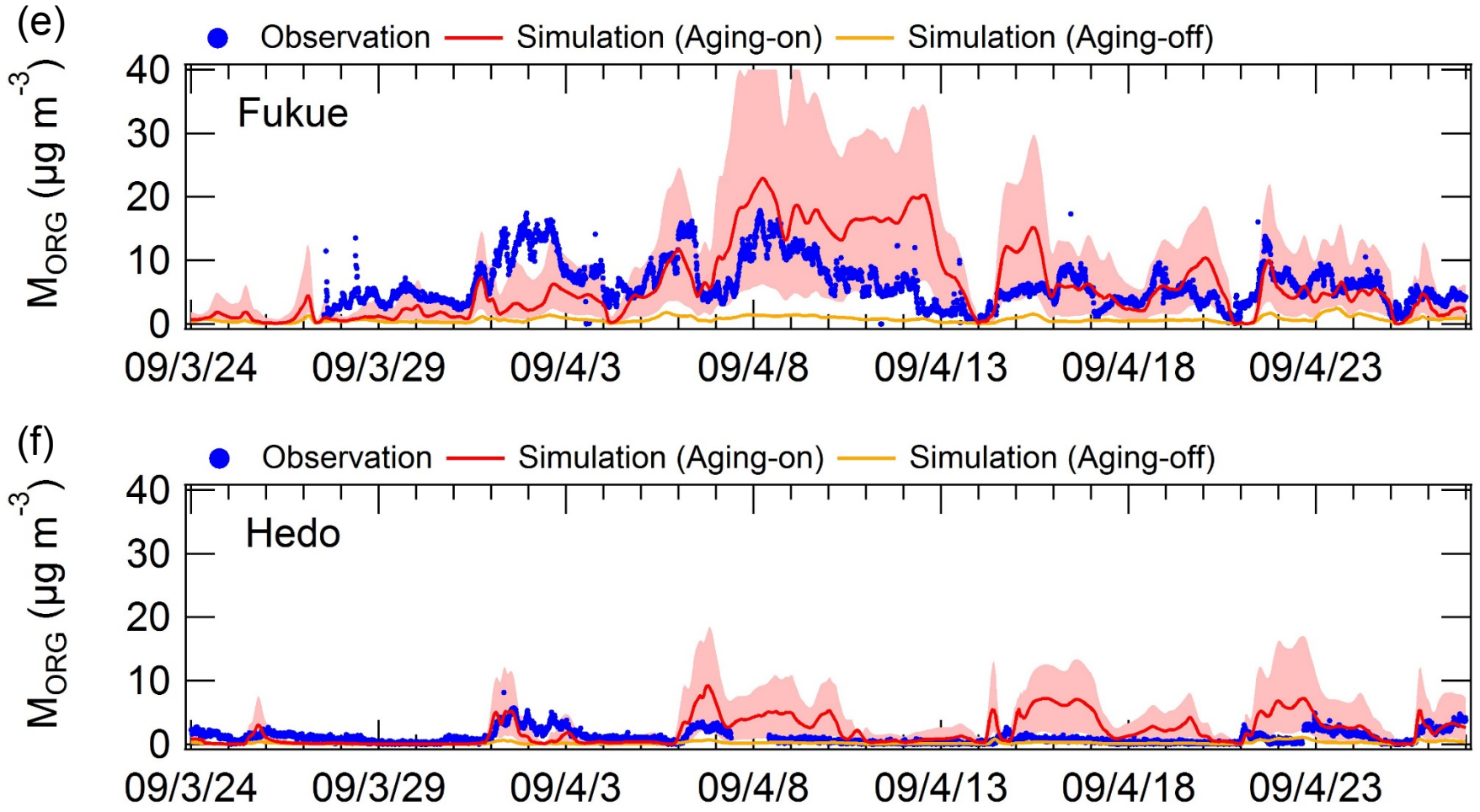
(e)
Observation
Simulation (Aging-on)
Simulation (Aging-off)
Fukue
M_{ORG} (μg m^{-3})
40
30
20
10
0
09/3/24
09/3/29
09/4/3
09/4/8
09/4/13
09/4/18
09/4/23
(f)
Observation
Simulation (Aging-on)
Simulation (Aging-off)
Hedo
M_{ORG} (μg m^{-3})
40
30
20
10
0
09/3/24
09/3/29
09/4/3
09/4/8
09/4/13
09/4/18
09/4/23

Fig. 6 (cont.)

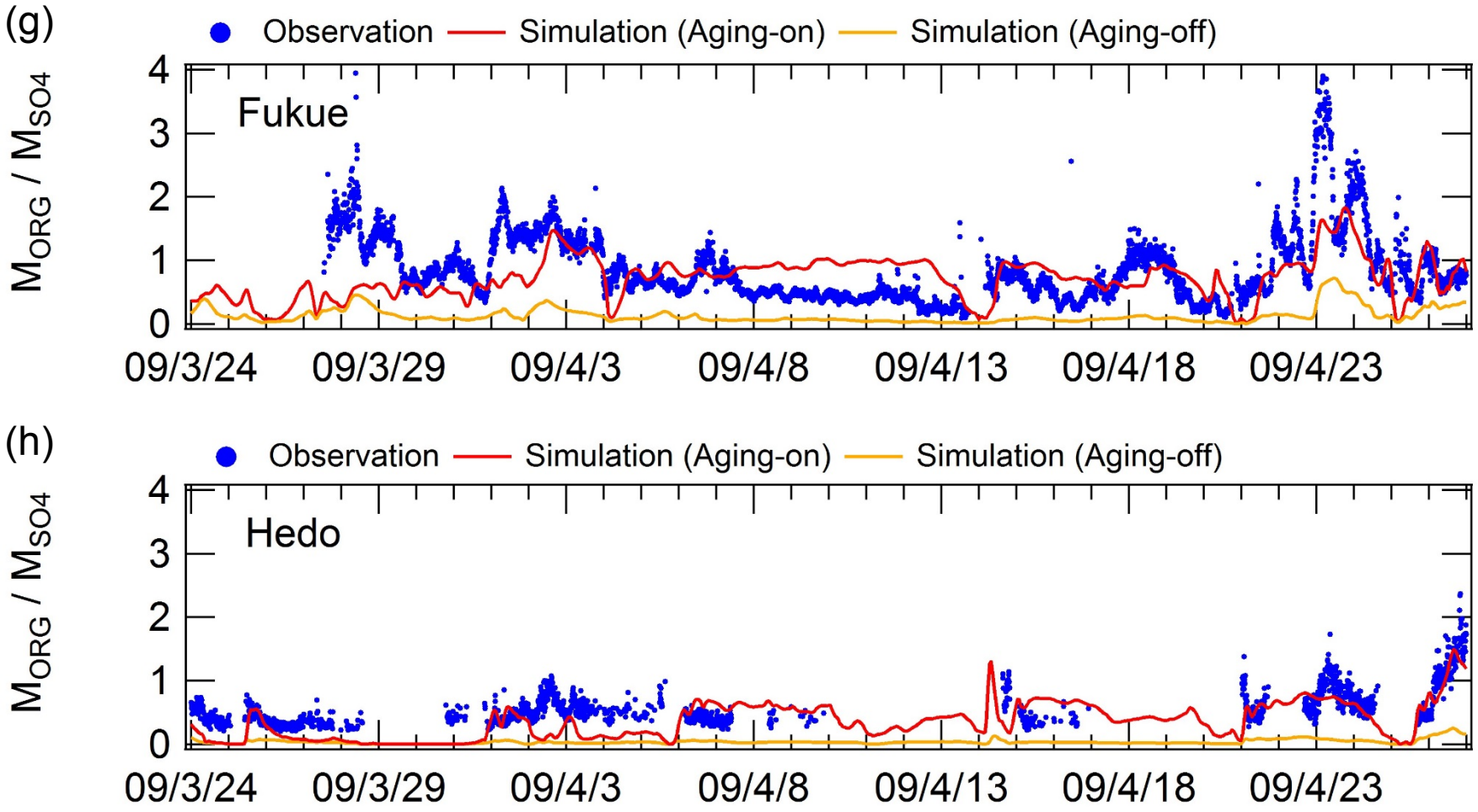
(g)
Observation
Simulation (Aging-on)
Simulation (Aging-off)
Fukue
M_{ORG} / M_{SO4}
4
3
2
1
0
09/3/24
09/3/29
09/4/3
09/4/8
09/4/13
09/4/18
09/4/23
(h)
Observation
Simulation (Aging-on)
Simulation (Aging-off)
Hedo
M_{ORG} / M_{SO4}
4
3
2
1
0
09/3/24
09/3/29
09/4/3
09/4/8
09/4/13
09/4/18
09/4/23

Fig. 7

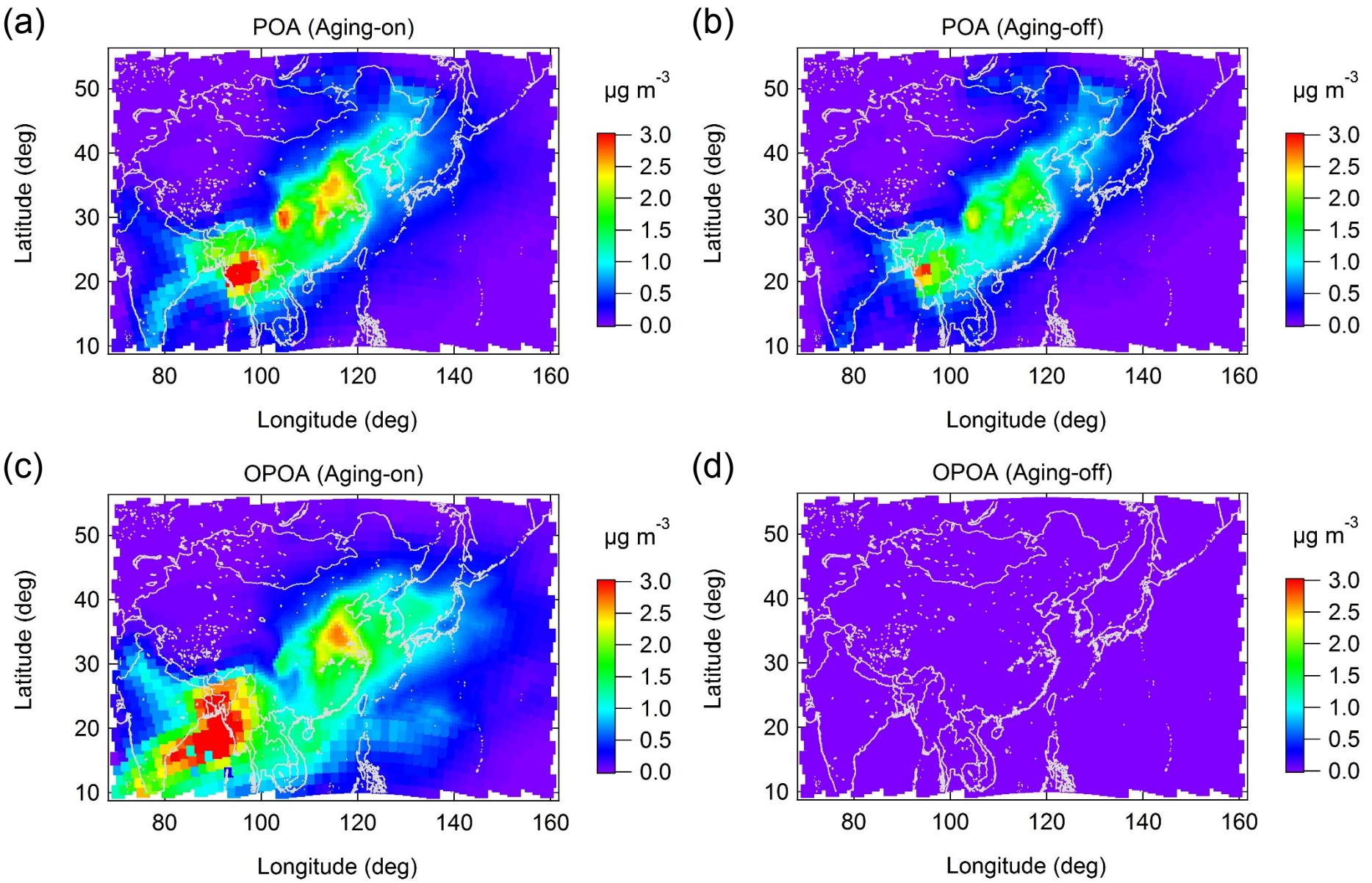
(a)
POA (Aging-on)
(b)
POA (Aging-off)
(c)
OPOA (Aging-on)
(d)
OPOA (Aging-off)
Latitude (deg)
Longitude (deg)
10
20
30
40
50
80
100
120
140
160
μg m-3
3.0
2.5
2.0
1.5
1.0
0.5
0.0

Fig. 7 (cont.)

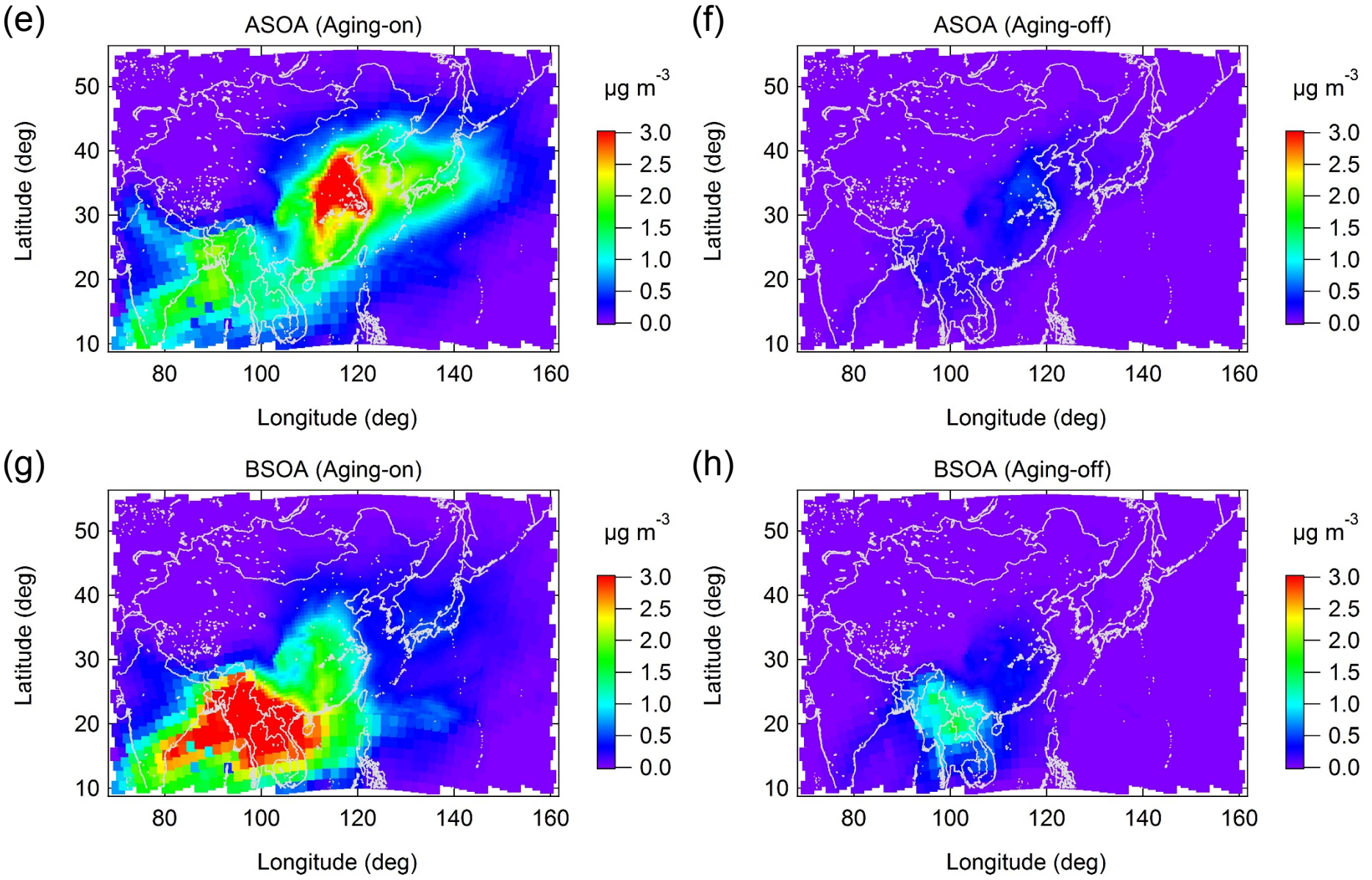
(e)
ASOA (Aging-on)
(f)
ASOA (Aging-off)
(g)
BSOA (Aging-on)
(h)
BSOA (Aging-off)
Latitude (deg)
Longitude (deg)
10
20
30
40
50
80
100
120
140
160
μg m-3
3.0
2.5
2.0
1.5
1.0
0.5
0.0

Fig. 7 (cont.)

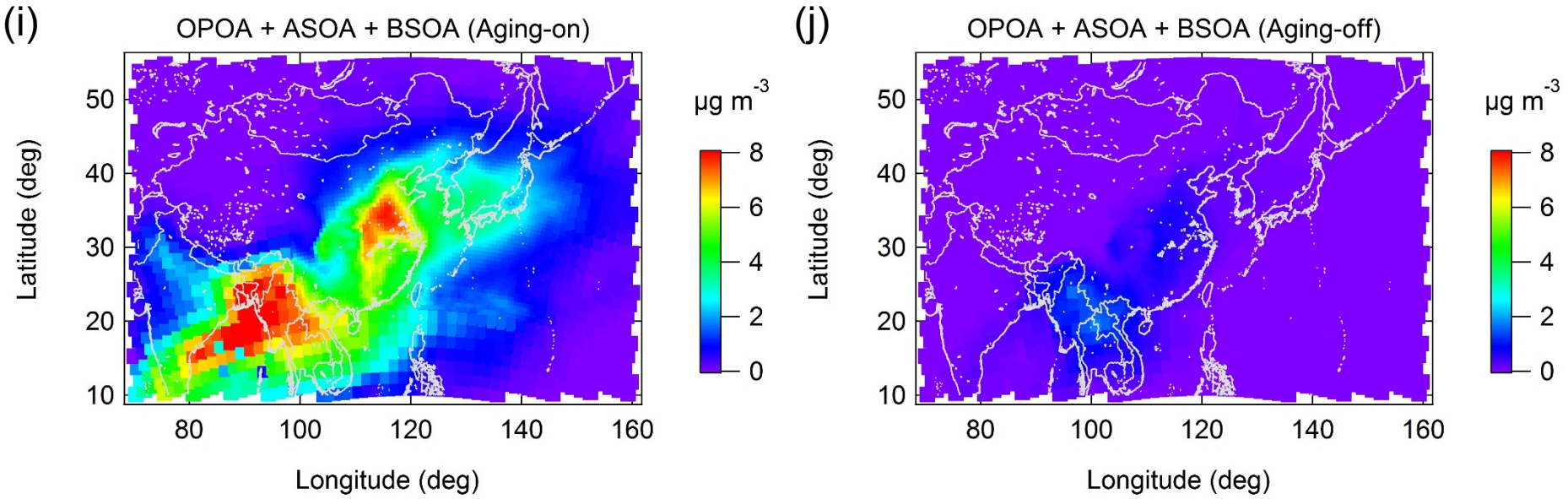
(i)
OPOA + ASOA + BSOA (Aging-on)
Latitude (deg)
Longitude (deg)
μg m-3
(j)
OPOA + ASOA + BSOA (Aging-off)
Latitude (deg)
Longitude (deg)
μg m-3

Fig. 8

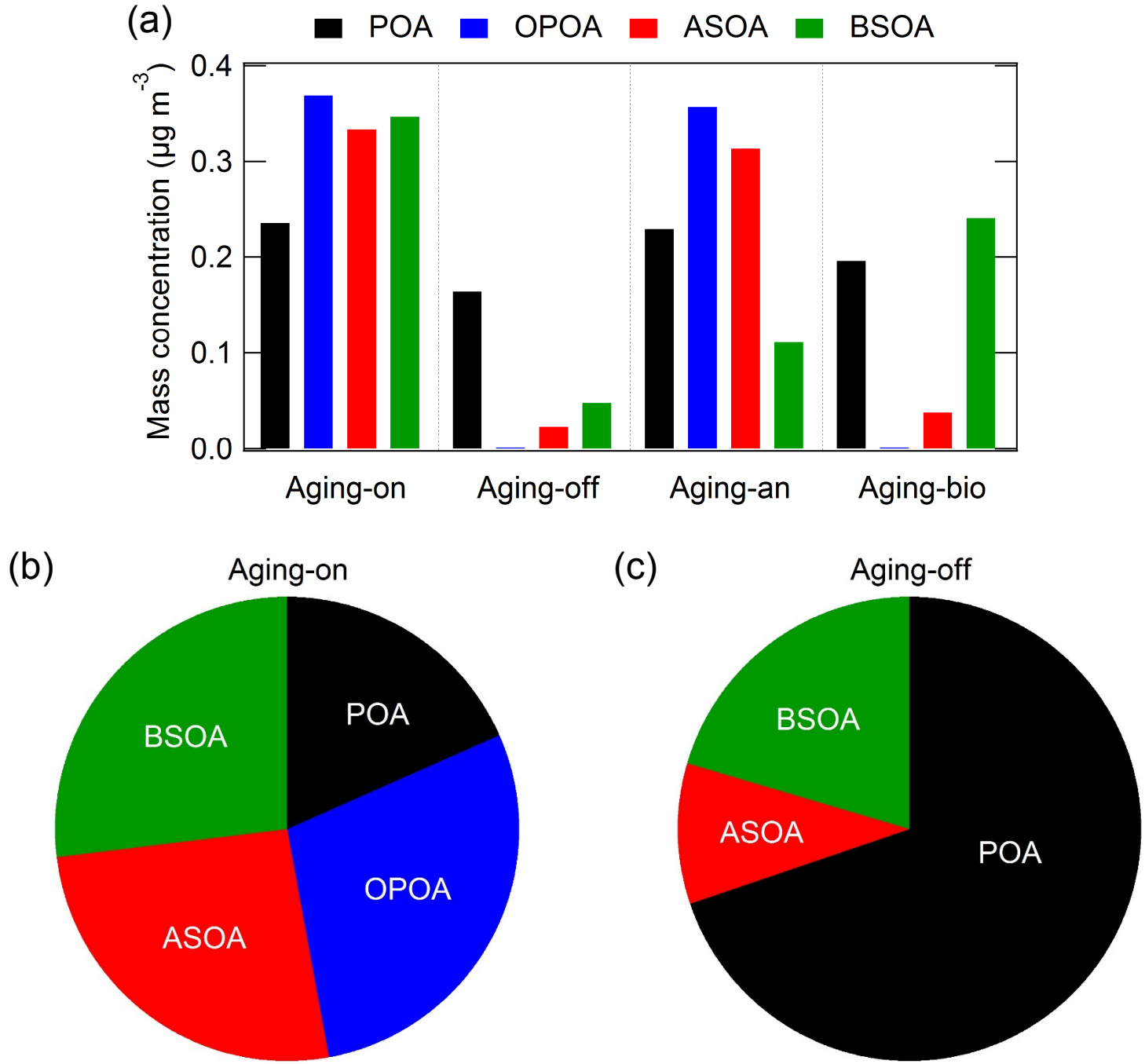
(a)
POA
OPOA
ASOA
BSOA
Mass concentration (μg m-3)
0.4
0.3
0.2
0.1
0.0
Aging-on
Aging-off
Aging-an
Aging-bio
(b)
Aging-on
BSOA
POA
OPOA
ASOA
(c)
Aging-off
BSOA
ASOA
POA

Fig. 9

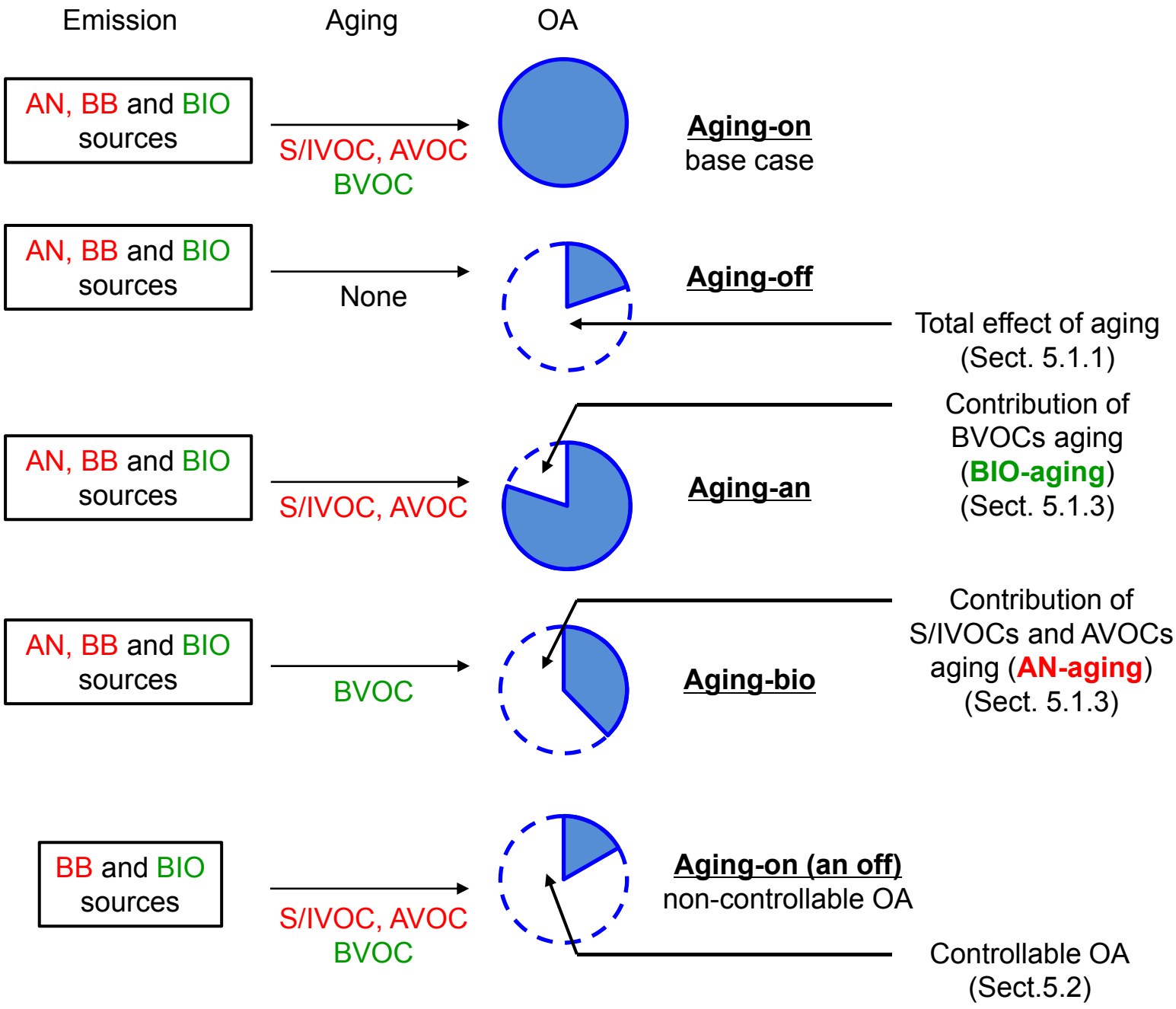
Emission
Aging
OA
AN, BB and BIO sources
S/IVOC, AVOC
BVOC
Aging-on
base case
AN, BB and BIO sources
None
Aging-off
Total effect of aging
(Sect. 5.1.1)
AN, BB and BIO sources
S/IVOC, AVOC
Aging-an
Contribution of BVOCs aging (BIO-aging) (Sect. 5.1.3)
AN, BB and BIO sources
BVOC
Aging-bio
Contribution of S/IVOCs and AVOCs aging (AN-aging) (Sect. 5.1.3)
BB and BIO sources
S/IVOC, AVOC
BVOC
Aging-on (an off)
non-controllable OA
Controllable OA
(Sect.5.2)

Fig. 10

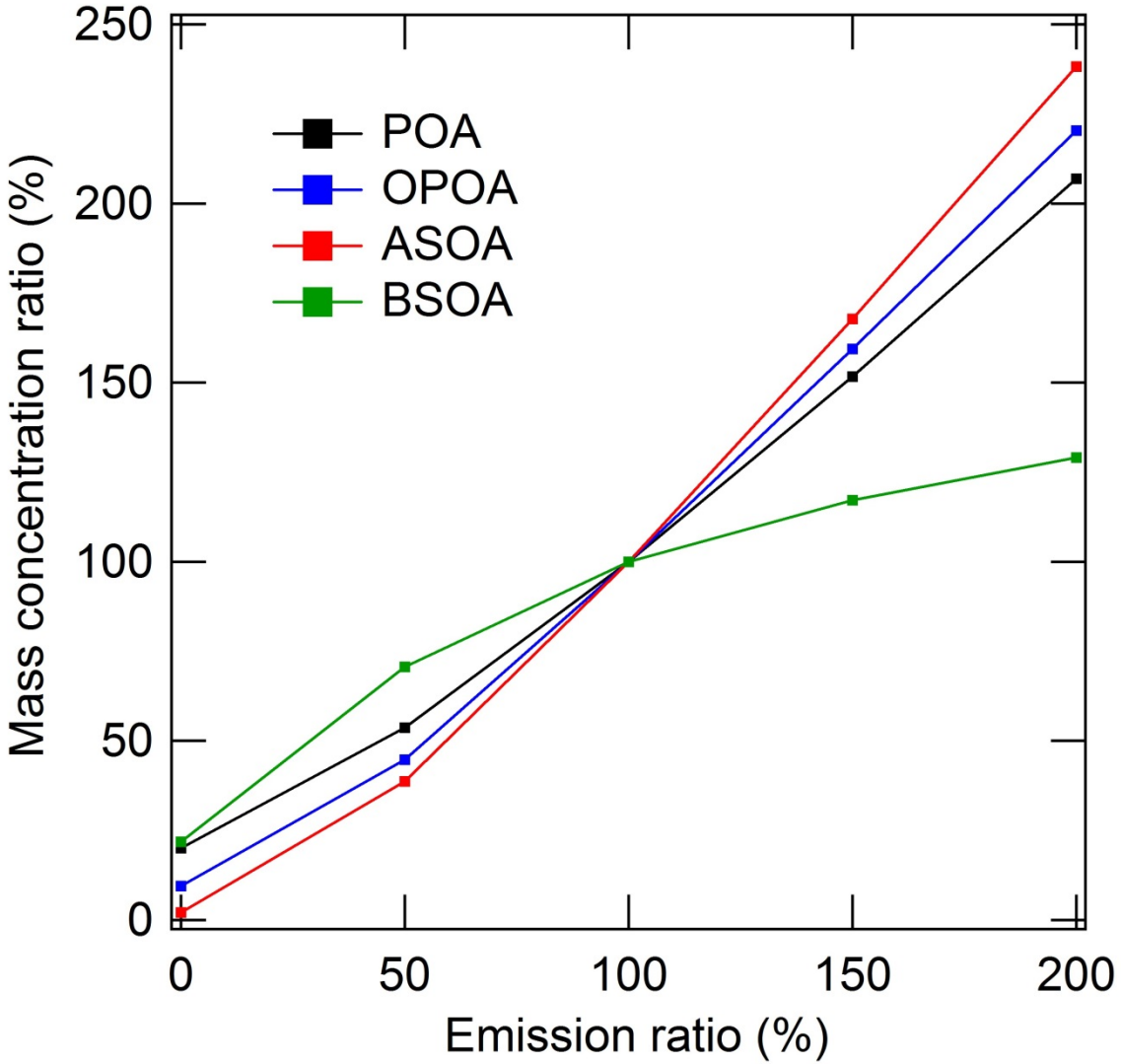
POA
OPOA
ASOA
BSOA
Mass concentration ratio (%)
Emission ratio (%)
0
50
100
150
200
250

Fig. 11

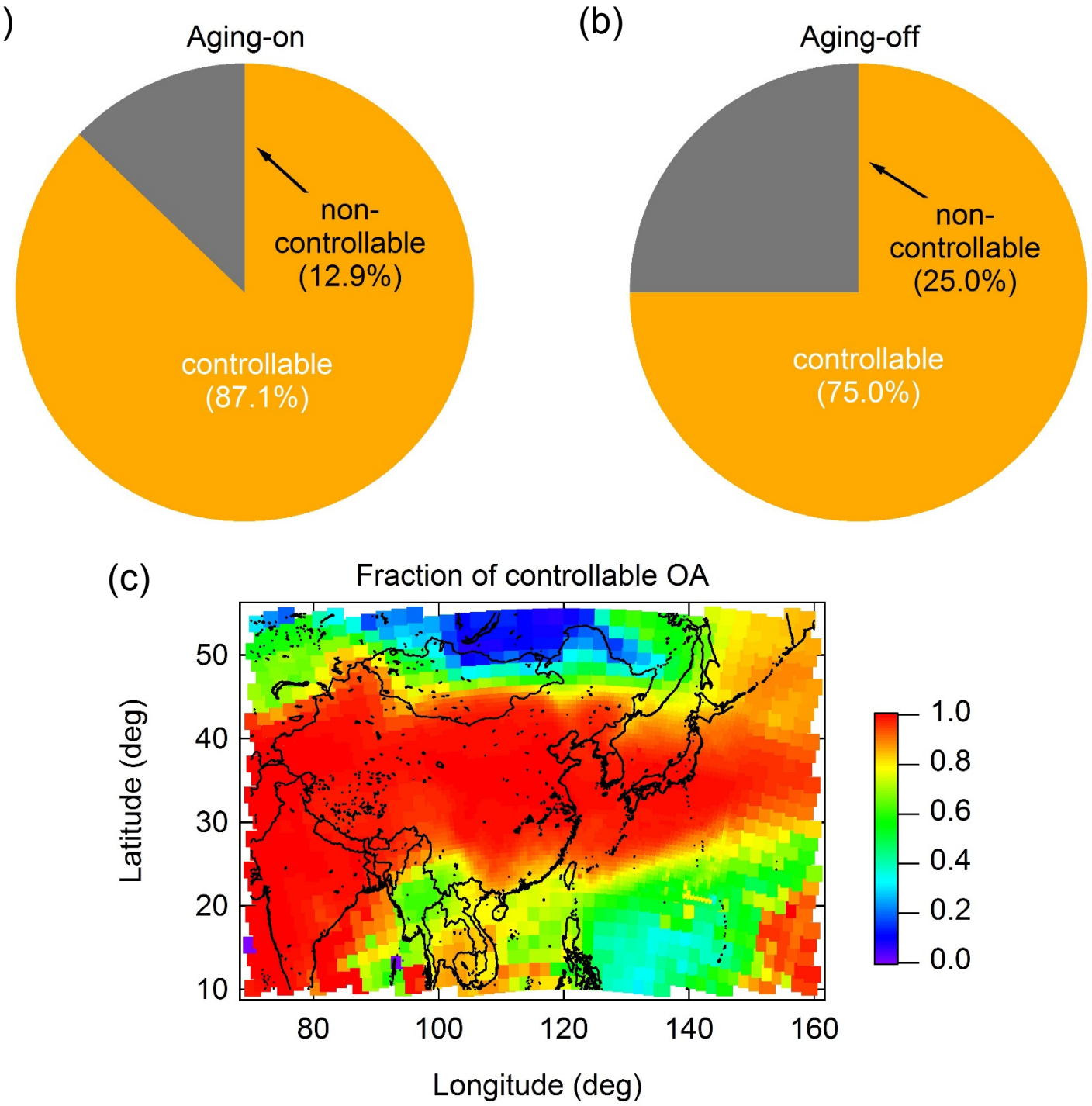
(a)
Aging-on
non-
controllable
(12.9%)
controllable
(87.1%)
(b)
Aging-off
non-
controllable
(25.0%)
controllable
(75.0%)
(c)
Fraction of controllable OA
Latitude (deg)
50
40
30
20
10
80
100
120
140
160
Longitude (deg)
1.0
0.8
0.6
0.4
0.2
0.0